Progress in Quantum Electronics xxx (xxxx) xxx

Contents lists available at ScienceDirect

Progress in Quantum Electronics

journal homepage: www.elsevier.com/locate/pqe

Optical characterisation of nanowire lasers

Stephen A. Church [a], Ruqaiya Al-Abri [a], Patrick Parkinson [a,*], Dhruv Saxena [b]

[a] Department of Physics and Astronomy and The Photon Science Institute, University of Manchester, Manchester, M13 9PL, United Kingdom
[b] The Blackett Laboratory, Department of Physics, Imperial College London, London, SW7 2BW, United Kingdom

ARTICLE INFO

Keywords:
Semiconductor lasers
Nanowires
Optical spectroscopy
FDTD simulation

ABSTRACT

Semiconductor nanowire lasers are single-element structures that can act as both gain material and cavity for optical lasing. They have typical dimensions on the order of an optical wavelength in diameter and several micrometres in length, presenting unique challenges for testing and characterisation. Optical microscopy and spectroscopy are powerful tools used to study nanowire lasers; here, we review the common techniques and analytical approaches often used and outline potential pitfalls in their application. We aim to outline best practise and experimental approaches used for characterisation of the material, cavity and lasing performance of nanowires towards applications in biology, photonics and telecommunications.

1. Introduction

Semiconductor nanowires are artificial nanomaterials with diameters typically between 10 and 1000 nm and lengths that can range between 1 and 100 μm. The wire-like morphology of nanowires combined with the high refractive index and high luminescence and optical gain of direct bandgap semiconductors lead to a variety of useful photonic properties, such as strong waveguiding, large polarisation anisotropy of absorption and emission, and lasing. The flat crystalline end facets of nanowires can also provide large reflection coefficients for guided modes [1], which enables single nanowires to function as standalone Fabry-Pérot type cavities, without any further fabrication processes. Lasing in nanowires can therefore be observed by optically pumping individual nanowires, such as in a micro-photoluminescence setup with a pulsed pump laser [2].Table 1
A list of parameters used in this review with their definition.

Symbol	Definition	Units
λ_0	Primary lasing peak wavelength	nm
l_c	Coherence length	m
L	Nanowire cavity length	m
P_{th}	Laser threshold (pulsed)	μJ cm^{-2}pulse^{-1}
	Laser threshold (continuous)	kWcm^{-2}
IQE (or PLQY)	Internal quantum efficiency (Photoluminescence Quantum Yield)	N/A
E_g	Material band-gap	electron volts (eV)
Σ	Non-thermal electronic disorder energy	electron volts (eV)
Γ	Optical confinement factor	N/A

(*continued on next page*)

* Corresponding author.
E-mail address: patrick.parkinson@manchester.ac.uk (P. Parkinson).

https://doi.org/10.1016/j.pquantelec.2022.100408

Available online xxxx

Table 1 (*continued*)

Symbol	Definition	Units
β	Fraction of spontaneous emitted light coupled to a laser mode	N/A
γ_p	Photon damping rate	s^{-1}
γ_{rc}	Radiative rate constant	s^{-1}
n	Refractive index	N/A
R	Reflectivity of nanowire facet	N/A
α_0	Distributed losses in the nanowire	cm^{-1}
g_{th}	Threshold gain for lasing	cm^{-1}
g_0	Differential gain coefficient	cm^3s^{-1}
Q	Nanowire cavity quality factor	N/A

The advancements in growth of semiconductor nanostructures over the last two decades has sparked significant scientific interest and research into nanowire lasers [3], some of which are shown in Fig. 1. Nanowire lasers have therefore been realised across many different material platforms, several of which were relatively unexplored because of difficulties in material growth and fabrication processes. Notably, nanowire growth has less stringent requirements on lattice matching to the growth substrate, and because of strain relaxation the nanowires can have reduced defect densities compared to bulk crystals [4–6]. In particular, the simplicity in forming the lasing cavity with nanowires compared to conventional planar semiconductor lasers (which require numerous fabrication steps) has enabled demonstration of lasing in a wide variety of gain materials - metal-oxides [7], chalcogenides [8], nitrides [9], III-V semiconductors [10] and more recently, perovskites [11]. Moreover, nanowires have opened up possibility of three-dimensional architectures [12] and high-density integration beyond what is possible with planar or top-down lithography.

Over the past decade, a number of review articles have been written about nanowires lasers in general [13–15], or applications in electrical pumping [16], specific materials such as nitrides [17], zinc oxide [7,18] or hybrid perovskites [19,20], dynamics [21], or silicon integration [22,23]. The present review seeks to focus on optical characterisation methods used to measure and compare nanowire lasers. We discuss techniques including computational modelling, photoluminescence spectroscopy, time-resolved spectroscopy and imaging in Section 2. Section 3 review optical methods to study the materials used in nanowire lasers, including heterostructures and doping. In Section 4 we discuss methods to characterise nanowire laser cavities for reflectivity and losses, before covering the characterisation of laser operation in Section 5. Finally we outline approaches to integration for nanowire lasers in Section 6 before providing a brief outlook in Section 7.

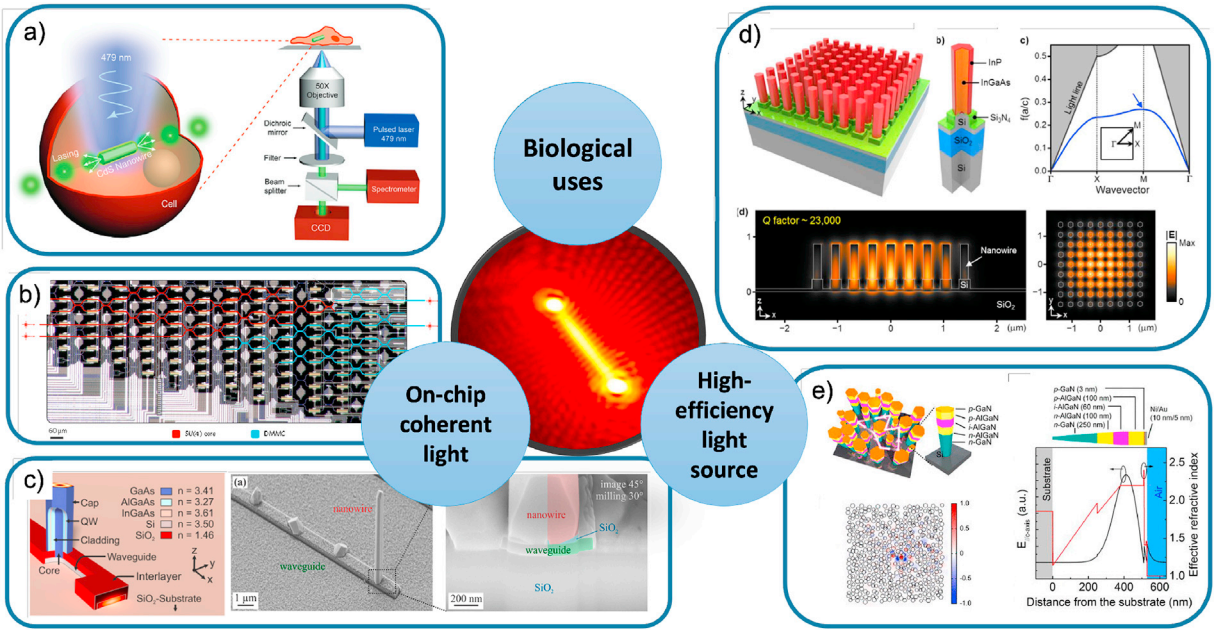

Fig. 1. Key applications for nanowire lasers include biological use, on-chip coherent light sources for photonic integrated circuitry and telecommunication wavelength integration, and high-efficiency silicon-integrable light sources. (a) Biological applications include intra-cellular use to sense small environmental changes [24]. (b) Small, integrated light sources are sought for coherent nanophotonics [25], particularly based on a silicon platform such as the photonic processor reported by Shen and colleagues. (c) One approach to integration is to grow nanowire lasers directly onto an on-chip waveguide [26,27], separating the lasing function from the computational components as shown by the Finley group (Reprinted with permission from ACS Photonics 2017, 4, 10, 2537–2543. Copyright 2017 American Chemical Society). High efficiency light sources at myriad emission wavelengths using novel materials are sought for on-chip emission. (d) Arrays of nanowires provide opportunities for photonic crystal construction and high emission intensity at telecommunications wavelengths [28], whilst (e) Deep-UV (239 nm) emission from nitride-based materials benefits from the nanowire architecture by minimising crystal defects [29].

1.1. Applications

To understand the characterisation needs for developing semiconductor nanowire lasers, we first consider potential applications and relevant figures of merit to be optimised. To date, the majority of research on nanowire lasers has been related to fundamental nanophotonics - understanding light-matter interaction at the nanoscale. Indeed, experimental work often linked to a number of pioneering theoretical works by Maslov and Ning [1,30–32] which sought to understand reflectivity and modal confinement at the nanoscale.

Many early applications of nanowires focused on biological applications in sensing [33–35], epitomised by research from the group of Peidong Yang who considered nanowires as optical probes for cellular endoscopy in 2011 [36]. Nanowires are small enough to penetrate the cell membrane allowing in-situ use [37], and a particularly striking application was reported by Wu in 2018, who proposed intra-cellular use of nanowire lasers; this made use of the non-linearity and sensitivity of lasers to their dielectric environment for application in pH sensing [24] as shown in Fig. 1a. In biological applications, a small diameter and length, a biologically inert material, and visible wavelength lasing are critical.

More recently, advances in growth has renewed interest in on-chip integration of nanolasers with heterogeneous substrates, with applications in photonic on-chip circuitry such as depicted in Fig. 1b. Over the past decade, the need for coherent light sources for next-generation photonic computing has grown due to the emergence of new photonic architectures [38,39]. This in turn has spurred research into nanowire lasers that can be grown directly onto silicon or optical waveguides (Fig. 1c). The Finley and Chang-Hasnain groups have made notable contributions in this area, demonstrating growth of high quality lasers on silicon [40], position-controlled growth [41] and coupled-growth on waveguides [26,27]. More recently the field has been accelerated by work on hexagonal structured silicon-germanium for direct bandgap emission [42] using group IV compounds. In applications for photonics, low-threshold, repeatability (inter-wire variance) and temperature stability are paramount.

The ability to grow heteroepitaxially whilst relieving strain has provided a third set of applications for nanowire lasers: in the production of high quality light sources using novel and emerging materials such as aluminium nitride or hybrid perovskites, or integration of established materials such as indium gallium arsenide (for infrared emission) with cheaper substrates. Deep-UV emitters based on AlN have been demonstrated by Zhao [29] for 239 nm emission, grown on silicon as shown in Fig. 1e. Telecommunication-wavelength lasers have presented a particular opportunity for nanowire lasers, where conventional flip-chip approaches to heterointegration can be complex and costly. Many groups have focused on the growth of telecommunication wavelength lasers onto silicon or waveguides, with the Huffaker group demonstrating array lasers [28,43,44] (see Fig. 1d) and Yokoo reporting hybrid nanowire laser-photonic crystal structures at telecommunication wavelength [45]. In this case, single-mode, narrow linewidth, precise wavelength, high total power and low-threshold operation are crucial.

1.2. Figures of merit

As can be seen, each application makes specific demands on the design and performance of nanowire lasers. Taken together, these form figures of merit - values that must be optimised during the design-growth-characterise cycle. These include:

Centre wavelength The lasing wavelength of a nanowire laser depends on the modal structure and spectral overlap with the gain curve. In long-cavity lasers this is typically determined by the gain spectrum; however, control of centre wavelength is often a challenge for short nanowire lasers (with widely space modal structure) or nanowires where compositional inhomogeneity is present [11].

Single/multi-mode operation Many applications, particularly those dependant on highly-coherent emission, require single-mode operation [46–48]. Nanowire lasers with short cavities provide widely spaced longitudinal modes which are better suited for single-mode operation, but thick wires can host a number of near-degenerate transverse modes. Cavity design is crucial to control the mode of operation.

Coherence length The coherence length of a nanowire laser is critical for use in photonic circuitry. Specifically, the coherence length must be on the order of the circuitry size; this is challenging for short nanowire lasers as it requires a high effective quality factor. High quality end-facets and low distributed losses have been shown to enable millimetre-scale coherence [49].

Pulsed/continuous operation Almost all conventional applications make use of continuously operating lasers. However, the relatively poor thermal stability of nanowire lasers (due to challenges with heat management at the micron-scale) has led to most wires being operated in a quasi-continuous regime. In some cases, pulsed or rapidly varying operation is actively sought [50]; here, strong coupling between optical and electronic modes in nanowires provide notable advantages over planar systems.

Lasing threshold Often the key figure of merit reported is the lasing threshold; the input power or energy required to induce lasing. The lower the threshold, the less pump power is required to generate lasing. This value is highly sensitive to the environment and experimental conditions. While very low values have been measured for perovskites [11,51] or at low temperature [52], room-temperature and statistically reproducible values are often sought [49,53].

Damage threshold and thermal stability Laser operation at room-temperature or above is essential for real-world applications. Materials with enhanced stability are often sought amongst inorganic materials [54], however some progress has been made with hybrid perovskite nanowire lasers [55] through compositional tuning.

Yield and reproducibility While control over all parameters have improved over the past two decades, it is notable that studies of yield (the fraction of nanowires which show lasing) and reproducibility are less common. Industrial applications which require integration must consider the spread in performance [53,56], and the impact of integration and fabrication steps upon this [57,58].

2. Techniques

Regardless of the material and geometry employed, efficient semiconductor nanowire lasers are typically based on high radiative rate materials with low-loss cavities. A wide range of materials and photonic characterisation techniques exist to study critical parameters such as internal quantum efficiency (IQE), photon and carrier dynamics, cavity modal structure and losses, however, care must be taken applying these to wavelength-scale cavities. Central to this is the challenge in measuring and calculating cavity properties from precise geometrical studies of the nanowire cavity itself; in conventional macro-scale laser design, the cavity can often be produced to an exceptionally high level of precision. For nanowires, we are not able to impose specific geometries with ease, and it is hard to measure and correlate this with individual laser performance.

The combination of unintentional wire-to-wire variation in geometry [59,60] with the highly non-linear relationship between reflectivity and shape [1] mean that attention must be paid to the implementation of techniques used, simulation and modelling, and multiple measurements for statistically significant characterisation. In this section, commonly used experimental and modelling techniques are introduced and reviewed.

2.1. Numerical modelling

Modelling of nanophotonic structures has become an essential part of scientific research - to support experimental observations, aid physical understanding and for optimising design [63]. For nanowire lasers, numerical modelling is often used, as analytical solutions are not always possible. There are two popular numerical methods for solving Maxwell's equations: finite element (FE) and finite-difference time-domain (FDTD). FE method solves equations in the frequency domain and is better suited for finding eigenmodes and estimating cavity Q factors whereas FDTD is a time domain method and is more suitable for broadband simulations such as scattering/absorption cross-section, reflection from an interface and far-field profiles.

One of the first steps in modelling nanowire lasers is determining the guided modes supported in the nanowire cross-section, as shown in Fig. 2a–c. The modes in a nanowire are similar to those in a cylindrical waveguide, and so the modes found using numerical methods can be named and identified from their field distribution, polarisation and effective index (dispersion) [61,64]. The calculation of the mode profiles, group and effective index from numerical simulations is very useful for determining mode confinement factors (Γ), axial mode numbers and mode spacing ($\Delta\lambda$) in lasing spectrum.

Apart from waveguide modelling for which eigenmode solvers or FE methods are used, the majority of other modelling problems require FDTD. Some of these are depicted in Fig. 2d–f, such as mode reflectivity at nanowire end-facets [13,18], the far-field emission profile [62] and mode coupling from nanowire into a waveguide [27], respectively. Typically 3D simulations have to be performed for such calculations, but structural symmetry of the nanowire can help to reduce simulation size and time. In general it is good practice to

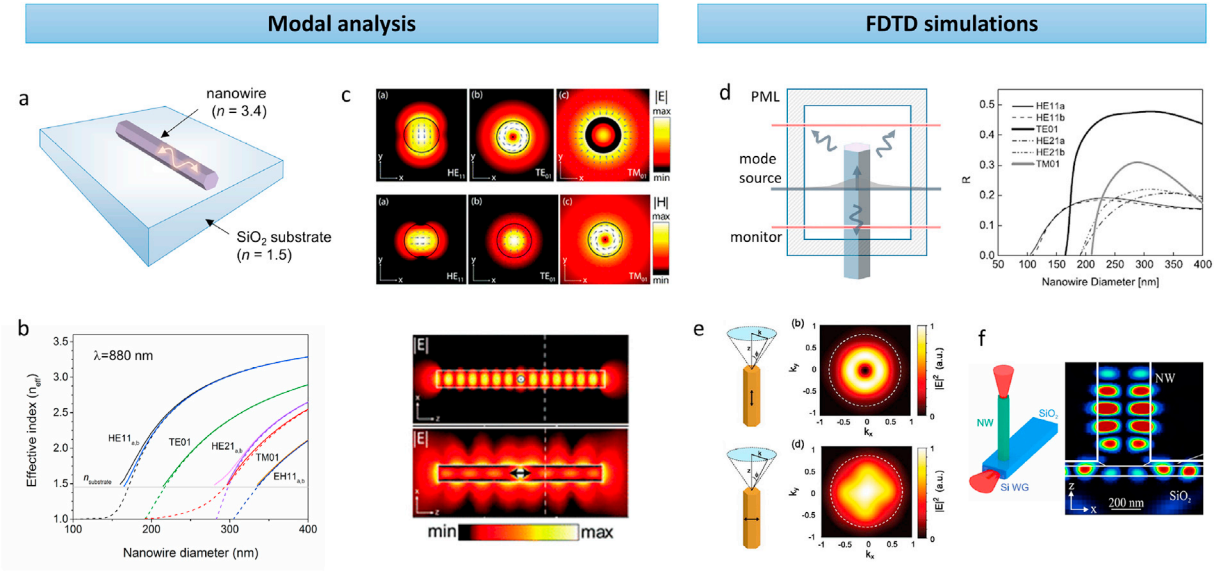

Fig. 2. Numerical modelling of nanowire lasers. (a) A typical arrangement for nanowire lasers has the nanowire lying horizontally on top of a low index substrate. Guided modes in the cross-section of the nanowire can be found through numerical methods. (b) Mode dispersion as a function of nanowire diameter [10]. (c) Electric and magnetic field profiles of the first few guided modes in the nanowire, with corresponding vector fields superimposed. Below the electric field in axial direction showing cavity resonances in the nanowire [61]. (d) Typical setup of a FDTD simulation to evaluate the mode reflectance from the nanowire/air end facet. Mode reflectance calculated from such simulations for a nanowire lying on SiO_2 substrate is shown on the right [18]. (e) Simulation of far-field emission profiles from nanowire end facet for a dipole emitter perpendicular or parallel to nanowire axis [62]. (f) Simulation of mode coupling in a nanowire integrated with a silicon waveguide [27]. (Reprinted with permission from ACS Photonics 2017, 4, 10, 2537–2543. Copyright 2017 American Chemical Society.).

check validity of simulations against theory (if available) or other published works and important to do convergence tests to ensure numerical results are not affected by simulation time span, domain size and mesh resolution.

2.2. Photoluminescence spectroscopy

Photoluminescence spectroscopy refers to the measurement of the intensity of light emitted from a material as a function of photon energy following optical excitation, which may also be measured as a function of excitation energy, emission polarisation or material temperature. In comparison to planar films, when studying nanowires as a gain material two additional features must be considered; wave-guiding of emission by the cavity [65], and wire-to-wire variation in material quality [59]. While ensemble measurements are useful to characterise a growth run, they suffer from emission dominated by the highest-emitting subset of wires and peak broadening due wire-to-wire variation and are not considered appropriate for laser studies. A notable exception to this is the case of array-based lasers, which we consider separately in Section 6.2.

2.2.1. Semiconductor photoluminescence

Photoluminescence emission from a semiconductor designed for lasing typically originates from band-to-band recombination from close to the conduction band minima to the valence band. Measurement of the low-fluence emission – defined as a fluence where behaviour is carrier density independent – can be used to find the effective band-gap of the emissive material (for composition determination) [66], the effective electronic temperature [67], disorder (such as structural disorder [68]), doping [69], defect-related emission [70], excitonic binding energy [71] and quantum structure dimension [72], strain [73] and composition [49]. Modelling of emission ranges from simple, such as the fitting of a Gaussian or Lorentzian peak to an emission spectrum, through to use of semi-empirical models such as convoluted Boltzmann [53] or the Lasher-Stern-Würfel model (LSW) [42,74,75], through to a full quantum mechanical treatment. These models fit the emission spectrum as a function of energy using increasingly complex forms. For broad emission lines, often a simple Gaussian is used:

$$I_{PL}(\sigma, E_g) = A\exp\left(- \left(E - E_g\right)^2 \Big/ 2\sigma^2 \right) \tag{1}$$

where E_g is the centre of the emission linked to the band-gap of the material and σ is the related to the width of the peak. This approach assumes symmetric emission around the band-edge, which may be realistic in the case of highly-disordered material at high temperatures. Conversely, the emergence of an amplified spontaneous or lasing peak can often be modelled as symmetric where the linewidth originates from the laser cavity; for an ideal cavity with a high quality factor (Q-factor) the lineshape is best described by a Lorentzian where

$$I_{PL}(\sigma, E_g) = \frac{A}{\pi} \frac{\frac{1}{2}\sigma}{\left(E - E_g\right)^2 + \left(\frac{1}{2}\sigma\right)^2}, \tag{2}$$

although practical measurement constraints often result in a Gaussian-like line shape. In this case the emission Q-factor is given by $Q = \frac{E_g}{\Delta E}$ where ΔE is the full-width of the emission at half-maximum height. It is notable that the Q-factor of a cavity is best measured during amplified spontaneous emission, where the cavity properties dominate; measurement of Q-factor during lasing is not representative of the cavity itself and more details are given in Section 4.1. While the Gaussian and Lorentzian shapes are useful for either crude or high-Q emission, they are a poor choice for typical semiconductor emission. A comprehensive discussion is beyond the scope of this review but is covered in great detail elsewhere [76]. A number of semi-empirical approaches to modelling photoluminescence have been used for nanowire emission. By assuming that the density of state in the conduction band is smaller than in the valence band, thermal energy can be assumed to manifest as a broadening in electron energy and hence recombination energy. By convoluting a Boltzmann distribution (for thermal broadening) with a Gaussian (representing disorder) the emission can often be well modelled by [53,72]

$$I_{PL}(\sigma, E_g, T) = A\left[\exp\left(- E^2/2\sigma^2 \right) \otimes \sqrt{E - E_g} \exp\left(- \left(E - E_g\right)/k_B T \right) \right], \tag{3}$$

where T is the effective carrier temperature. In the presence of defects within the band-gap, Urbach [68] developed a model which allows for an exponential distribution in density of states below the band-edge. This is more commonly observed in absorption than emission spectra [77]. Recently Fadaly and colleagues have used the LSW model to describe emission from novel hexagonal (wurtzite) nanowires [42]. In this model, the emission is described as a function of the absorption using a thermodynamic approach described by a chemical potential [74],

$$I_{PL}(a) = \frac{2\pi}{h^3 c^3} \frac{E^2 a(E)}{\exp\left(\frac{E - \Delta\mu}{k_B T}\right) - 1}. \tag{4}$$

Here $a(E)$ is the absorption coefficient for the material and $\Delta\mu$ is the chemical potential of radiation. The choice of model for photoluminescence is often driven by the parameters to be determined, the quality of the data, or simply the complexity required to represent the photoluminescence. One notable issue can arise in the determination of the band-gap; it is notable that models that do not take temperature into account tend to over-estimate material bandgap energy by a value on the order of $k_B T$.

Since the work of Kroemer [78] and Alferov [79], heterostructuring and quantum-confinement have become a standard approach to tune the emission wavelength and increase the IQE of emission. Fig. 3b shows the emission spectrum for a typical quantum well nanowire system [53], an architecture that has been studied since the 2008 report of a multiple-quantum well GaN-based nanowire system by Qian [80]. Photoluminescence in these systems can be modelled using much the same approach as described above; however, the density of states term in equation (3) ($\sqrt{E-E_g}$) must be modified in the case of quantum wells (to be a constant) [72]. More details for characterisation of quantum structures are given in Section 3.2.1.

2.2.2. Power-dependent photoluminescence

For materials characterisation it is preferable to use low-fluence optical excitation to avoid carrier-carrier, non-linear optical or trap saturation effects. This is particularly the case for low-volume nanomaterials, however, many conventional optical techniques require high excitation density to achieve sufficient signal to noise ratio; these include transient spectroscopy [81], terahertz spectroscopy [82] and even photoluminescence at low temperatures [83]. For lasing studies however, we are expressly concerned with emission at high carrier densities where population inversion can be achieved. A typical study is a power-dependent photoluminescence measurement, where the emission is measured as a function of excitation (pump) power or pulse energy, as shown in Fig. 3d. An evolution in emission is observed with increasing power from equilibrium emission described above through to hot-carrier emission – due to state-filling leading to a blue-shift in emission – followed by amplified spontaneous emission with the emergence of wave-guided modes and a super-linear increase in output, and lasing where narrow emission lines dominating over spontaneous emission and a linear increase in integrated intensity [84].

The interpretation of fluence-dependent photoluminescence is central to laser characterisation. This experiment is visualised in two plots; complete emission spectra as a function of incident pump fluence, and extracted parameters such as integrated emission intensity or emission linewidth (full-width at half-maximum). The former, shown in Fig. 3 is used to illustrate spontaneous emission clamping – where emission away from the laser line saturates as any further increase in injected energy is directed into the lasing mode – as well as the onset of lasing and the onset of multi-modal emission. A plot of integrated emission intensity as shown in Fig. 3e provides quantitative information about the regime of operation, which gives rise to the characteristic “s-curve”. While the numerical value of this curve depends on many specific experimental parameters, the shape can be used to identify the approximate onset of amplified spontaneous emission and lasing (approximately at the first and second turning points, respectively) as well as the β-factor, which describes the coupling of energy into the lasing mode [40]. The modelling of threshold is described in more detail in Section 5.1.1.

2.2.3. Experimental arrangement

Photoluminescence spectroscopy of nanostructures requires microscopic spatial resolution to address single structures and identify

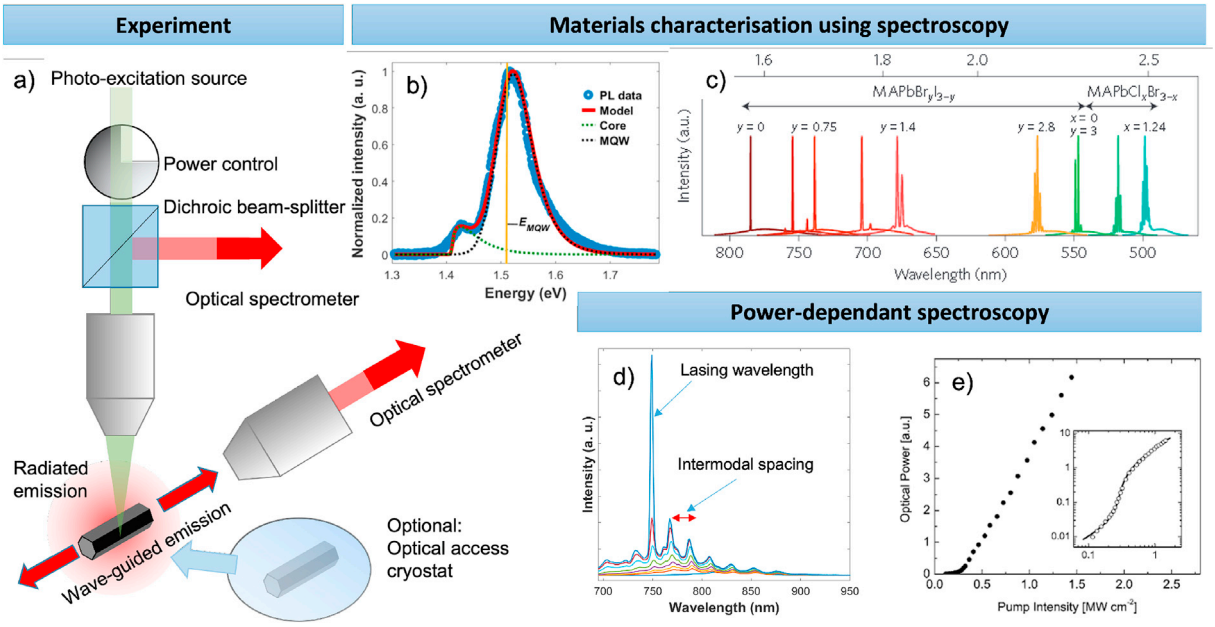

Fig. 3. Micro-photoluminescence spectroscopy of nanowires. (a) A typical experimental arrangement for micro-photoluminescence measurements on single nanowire lasers, depicting radiated and guided collection modes. Spectroscopy for materials characterisation, through (b) spectral modelling of photoluminescence emission [53] (Reprinted with permission from Nano Lett. 2017, 17, 8, 4860–4865, Copyright 2017, American Chemical Society) and (c) compositional determination in perovskite alloys [11]. (d) Power-dependant spectroscopy for laser characterisation, with key measurements (lasing wavelength, intermodal spacing) labelled. (e) The integrated emission as a function of excitation fluence is used to determine laser threshold through the charateristic ”s-curve“ (inset) [93].

spatial variation in emission. Fig. 3 gives a depiction of two typical arrangements - collinear and non-collinear. In the former, nanowires are pumped and the emission collected using a single objective [2], while in the latter the emission is collected with a second - typically on-axis - objective [40,85]. Nanowires are frequently transferred from their growth substrate to an inert carrier, to reduce their density and to provide high refractive index contrast at their base [60] (see Section 4.1). An exception to this is where the nanowire is grown onto a waveguide [27,44] or transferred onto one [86], where emission from the waveguide is typically probed. Low-index substrates, including indium-tin-oxide (ITO) coated glass have been used to avoid modifying the optical confinement of the nanowire laser [10] while providing good thermal conductivity.

The pump beam can be continuous wave or pulsed; in the former, an equilibrium carrier density is achieved, whilst in the latter the emission will vary as function of time after excitation leading to the observed photoluminescence being averaged. Continuous operation is sought-after, however pulsed operation often provides an easier route to achieving population inversion without risk of material damage through prolonged heating. Quasi-continuous operation provides a compromise where pulsed excitation is used with the pulse duration exceeding the carrier and cavity photon lifetime – typically in the nanosecond range – leading to the majority of the operation in the equilibrium regime, such as used by Guilhabert and colleagues [87].

The key specifications of the pump laser are photon energy [49], the beam polarisation (which determines the coupling strength to the nanowire), the pulse duration (the relationship to the photon cavity lifetime determines whether the laser operates in a pulsed or quasi-continuous mode), the spot size at the nanowire (which determines whether the wire has homogeneous gain or localized pumping which can be used for tunable emission [88]) and the incident power or fluence. Varying the latter provides a route to measurement of the lasing threshold, and measurement of the spot-size and pulse energy is critical to accurate determination. Spot-size can be measured using a travelling razor blade or an imaging method.

For lasing studies, the pump photon energy can have a profound effect on the lasing threshold and gain [49]. Having a photon energy close to the bandgap aids in reducing thermal heating, and may therefore reduce the threshold. However, in this configuration, increasing the pump fluence may generate a carrier density high enough to increase the quasi-Fermi energy separation to above the photon energy - thereby rendering the nanowire transparent at these energies, and saturating the lasing intensity [89]. High degrees of *p*-doping can achieve a similar effect due to the Burstein-Moss effect, resulting in partial filling of the valence band [89].

For generic nanowire studies, a common optical arrangement would be for a nanowire lying flat on a low-index substrate in air to be excited using a randomly or circularly polarised laser which is defocussed to cover the entire nanowire. The laser spot should be spatially homogeneous, giving uniform excitation across the nanowire.

2.2.4. Classical and non-classical emission

Isolating the lasing emission from amplified spontaneous emission and photoluminescence can be challenging without the use of time-resolved techniques [49] as discussed in Section 2.3. Definitive evidence for lasing can be challenging to establish, particularly in high-β devices. In this case, a combination of power-dependent photoluminescence (with spontaneous emission clamping, a characteristic “s-curve” and line-width narrowing), can be combined with photon-correlation measurements such as Hanbury-Twiss-Brown correlation to reveal a classical to bunching to classical transition, with the bunching regime corresponding to amplified spontaneous emission [40,90]. Additionally far-field measurements show changes in the emission pattern, as discussed in Section 2.4.

2.2.5. Summary

Photoluminescence spectroscopy is a key tool to measure the bandgap, material disorder, electronic temperature and indeed relative quantum efficiency of emission. With appropriate modelling, it has also been used to study doping in semiconductors [69,91] which can give rise to band-gap narrowing as discussed in Section 3.3. However, significant challenges exist; the small physical volume of nanowires coupled with high non-radiative rates in unpassivated structures [92] can lead to negligible emission at room temperature, and the high carrier density required for lasing studies often necessitates the use of pulsed femtosecond excitation and subsequent ultrafast dynamics. As such, time-resolved techniques are often preferred for quantitative measurements.

2.3. Time-resolved spectroscopy

Lasing requires a dynamical balance between carrier creation and photon emission. As the length-scale of the gain material and cavity are reduced, the time-scales involved in this equilibrium are reduced. Under short-pulsed excitation, the carrier density and photon populations do not reach an equilibrium and a host of ultrafast dynamical processes can be observed. A detailed review of these dynamics has been produced by Röder and Ronning [21]; what follows focuses on the measurement and interpretation of experimental findings.

For time-resolved measurements, a short pulse is required to create a non-equilibrium carrier density. This pulse should be approximated as a Dirac δ-function when compared with carrier diffusion, recombination or photon emission processes, and typically a sub-picosecond pulse is used. Following excitation, carriers are created, which cool rapidly (over the sub-picosecond to hundreds of picosecond timescale [96,97]). If excitons are created, these can undergo dephasing over sub-picosecond timescales [98]. Over the next few picoseconds, carriers can diffuse (from tens of nanometres to a micron [99]), form excitons (if energetically favourable) or reach trap-states [100]. Carriers can also recombine radiatively or non-radiatively; initially, we assume a negligible photon density within the cavity, so emission is spontaneous, which may or may not couple to a confined mode of the cavity.

2.3.1. Carrier and photon dynamics

The relative population of carriers N and photons S within the cavity are often described in terms of a coupled rate equation [101,

102]:

$$\frac{dS}{dt} = \Gamma g_0(N - N_0)S - \gamma_p S + \gamma_{rc}\Gamma\beta N \tag{5}$$

$$\frac{dN}{dt} = G(t) - \gamma_{rc}N - g_0(N - N_0)S, \tag{6}$$

where Γ is the modal confinement factor, g_0 is related to the gain coefficient of the material, N_0 is the transparency carrier density, γ_p is the cavity photon rate, γ_{rc} is the radiative rate and β is the spontaneous emission factor linking emission to coupling to the laser mode. Additionally, $G(t)$ is a generation rate for carriers, which is linked to the excitation pulse. This approach is valid for a single emissive mode, but must be modified in the case of multi-mode operation or in the case of multiple carrier types.

Measuring the carrier density and the emitted photon rate as a function of time provides a facile route for measuring physically important parameters such as γ_p which are otherwise challenging to assess (as described in Section 4.1). For small and relatively low-quality cavities such as that provided by a nanowire laser, cavity lifetime can be on the order of a few picoseconds [21], although longer lifetimes and significantly longer emission dynamics have been demonstrated to many nanoseconds in duration [49]. It is notable that emission dynamics need not be monotonic; a recent study by Thurn has demonstrated that very high frequency oscillations (> 100GHz) can occur in nanowire architectures arising from dynamic competition between heating and cooling [50].

2.3.2. *Experimental arrangement*

Three experimental types are typically used to probe these dynamics, as shown in Fig. 4: picosecond time-resolved emission including time-correlated single-photon-counting (TCSPC) [49], pump-probe techniques including two-pump methods [50,94,98], and ultrafast techniques such as Kerr-gating spectroscopy [95] or transient reflectivity [103]. Picosecond dynamics are well suited to low-fluence emission with relatively slow dynamics, as the TCSPC technique is often limited to timescales greater than 30 ps, although this approach provides an additional opportunity to integrate Hanbury-Brown-Twiss photon-bunching measurements (see Section 2.2.4). This technique is typically carried out in a similar arrangement to standard photoluminescence spectroscopy (see section 2.2), but using a TCSPC detection apparatus. The same results can also be achieved using a streak-camera detection for resolution down to 2 ps. Detection of infrared emission requires non-silicon based detectors, and InGaAs and superconducting detectors are now emerging tools for this range.

Ultrafast spectroscopic techniques are ideal for studying femtosecond to nanosecond dynamics, where non-linear and scattering effects may dominate [95]. This is particularly important for very short pulse emitting systems, such as poor quality materials that depend on fast radiative recombination [104] for efficiency. To achieve such short time resolution, optical methods for gating the emission must be used, such as fluorescence up-conversion spectroscopy [105] or Kerr-gating [106]. In both cases, an ultrafast pulse is split into two beams using a beam splitter, with one termed the pump and the other termed the gate. The pump is used to photoexcite the

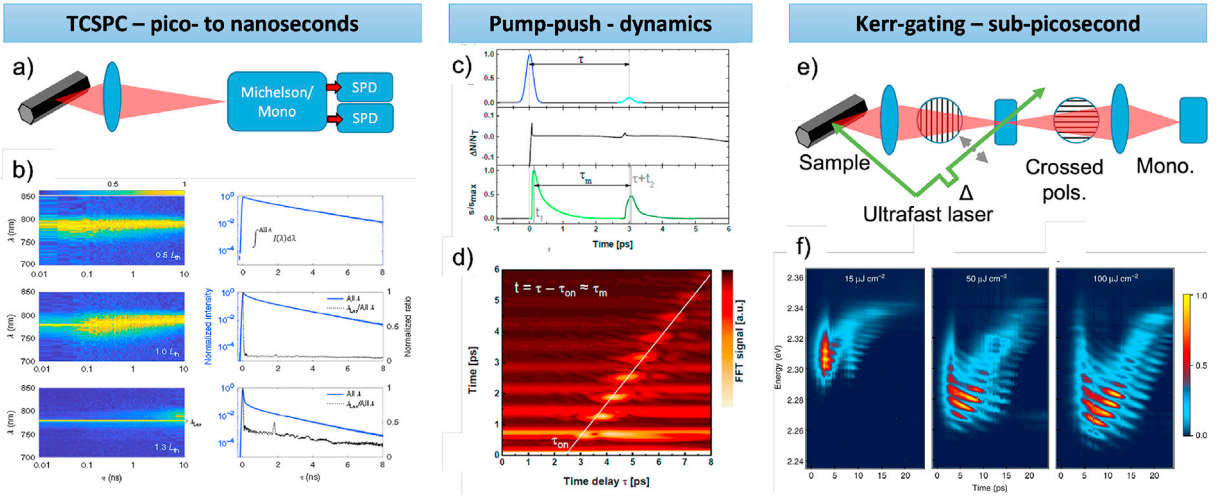

Fig. 4. Time-resolved spectroscopic techniques provide dynamical information of nanowire laser operation. (a,b) Time-correlated single photon counting (TCSPC) can be used with spectral resolution to provide emission dynamics on the ~10 ps to microsecond timescale [49]. This timescale is matched to carrier recombination times in high quality materials, and is best suited to study of photoluminescence. (c) Pump-pump methods can be used to determine the photon cavity lifetime, by determining the coherence of emission due to two temporally separated pulses [94] (Reprinted with permission from Nano Lett. 2015, 15, 7, 4637–4643, Copyright 2015 American Chemical Society). (d) A Fourier transform of the collected emission provides the onset time (related to carrier cooling) and the coherence time. (e) Ultrafast Kerr-gating spectroscopy provides time and energy resolved emission with sub-picosecond resolution. (f) It has been used to study the dynamics of laser emission from $CsPbBr_3$ nanowire lasers, linked to dynamic changes in refractive index and carrier cooling [95].

sample, and photoluminescence is collected via low dispersion optics (such as reflective optics) and focused to a gating material. The intense gate pulse is aligned coincidently with the photoluminescence on the gating material, generating a non-linear process which affects only the photoluminescence photons in the gating material during the gate pulse. This creates an "optical shutter" effect, either through sum-frequency generation (in photoluminescence up-conversion) or using transient birefringence (in Kerr-gating), and the upconverted light (or rotated photoluminescence) can be filtered and measured using a spectrometer. In transient reflectivity, it is the reflectance of a sample that is monitored as a function of delay, which can provide information about non-emissive dynamics such as surface recombination [103].

The pump-probe method also utilises non-linear processes and two or three ultrafast optical pulses to generate time-resolution. However, in this case the non-linearity is within the nanowire itself, either in its coherent response [98,107] or the carrier-photon coupled bath. This technique first creates a carrier population in the nanowire, which evolves for a period τ before a second pulse arrives. The second, weaker probe pulse is typically chosen such that it is below the lasing threshold, but can "top-up" the carrier population if it arrives after a stronger initial pulse. This induces a second lasing pulse, which can interfere with the first pulse creating a characteristic spectral interference (see Fig. 4b). This approach is unique in providing a number of insights; the minimum delay to observe interference is the turn-on time of the laser, while the maximum delay is the time to pulse-end [21,50]. The two-pulse technique is a powerful method to understand dynamics within single nanowire laser structures.

2.4. Far-field and Fourier plane imaging

The polarisation and far-field intensity profile of light emitted from any laser are important characteristics for identifying the lasing mode. However, unlike conventional edge-emitting lasers or VCSELs, the light emitted from nanowire end facets is highly divergent because the guided modes are fully vectorial with large transverse k-components [13,30]. Subsequently this presents some challenges for characterisation, as only a fraction of the light emitted from the nanowires can be measured with limited numerical aperture (NA) microscopy techniques. Furthermore, the substrate or other dielectric structures surrounding the nanowire can modify the far-field patterns. For nanowires lying horizontally on a substrate, the substrate also physically restricts optical measurements to only be side-on [108]. To characterise the emission end-on from the nanowire, the nanowire has to be either vertically standing or

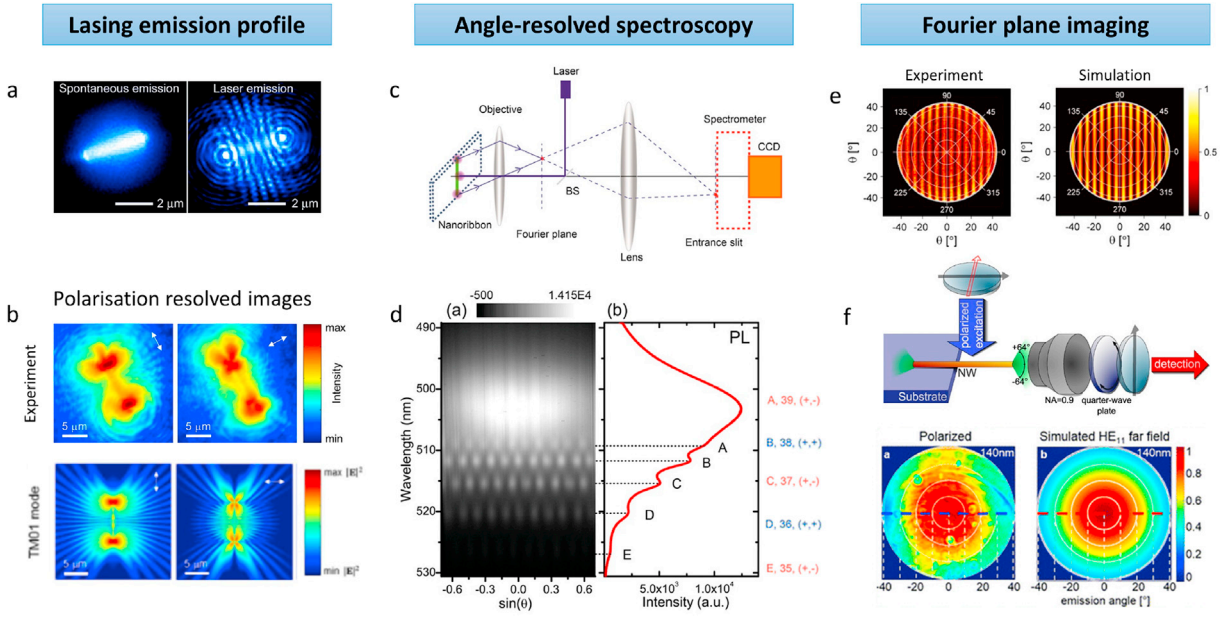

Fig. 5. Farfield and modal characterisation. (a) Optical images showing nanowire laser emission below and above threshold [109]. (Reprinted with permission from Nano Lett. 2006, 6, 12, 2707–2711. Copyright 2006 American Chemical Society.) (b) Polarisation resolved images may reveal distinct profiles that can help to identify which transverse mode is lasing by comparing with numerical simulations [108]. (Reprinted with permission from Nano Lett. 2015, 15, 8, 5342–5348. Copyright 2015 American Chemical Society.) (c–d) The axial order of the mode in the nanowire can be characterised by angle-resolved spectroscopy. In this method, the Fourier plane is imaged onto the spectrometer slit and the emission spectrally resolved. The spatially coherent emission from the two nanowire ends results in interference fringes, and the order and parity of the longitudinal mode can be inferred by fitting the fringe spacing [110]. (Reprinted with permission from Nano Lett. 2014, 14, 11, 6564–6571. Copyright 2014 American Chemical Society.) (e) Fourier plane image of nanowire laser emission and simulated far-field profile for TM01 mode. Here the nanowire is measured side-on [108]. (Reprinted with permission from Nano Lett. 2015, 15, 8, 5342–5348. Copyright 2015 American Chemical Society.) (f) An alternative approach to characterise far-field emission is to do head-on measurements. Here the nanowire is suspended from the edge of the substrate and the emission profile from one end-facet measured [85,111]. (Reprinted with permission from Nano Lett. 2016, 16, 4, 2878–2884. Copyright 2016 American Chemical Society.).

substrate-free. The latter can be achieved by suspending nanowire from the edge of a substrate by micro-manipulation or cleaving the substrate [85] (but the method is time consuming and not easy to extend for large number of nanowires).

Side-on measurement configuration for nanowire lasers, which is most common, can still provide substantial information for mode characterisation. Widefield imaging of nanowire lasers (with the pump laser filtered out) reveals different emission profiles below and above threshold [109]. Uniform emission from the body of the nanowire is typically seen for photoluminescence, whereas with the onset of gain and amplification of guided modes, bright emission from nanowire ends are observed. Distinct interference pattern is typically seen in widefield images when lasing emission from nanowire ends dominates, as in Fig. 5a.

Analysing the polarisation of emission from nanowire lasers and imaging the emission patterns with a polariser, as in Fig. 5b, can reveal distinct characteristics from which the lasing mode(s) can be identified [108]. This method requires comparison of mode profiles with simulations and so is most effective when the nanowire lasers are single mode and the end-facets are flat (so that the emission pattern is not distorted and can be well matched to simulations). The degree of polarisation, which defines how strongly polarised the emission is parallel or perpendicular to the nanowire axis, provides another metric for characterising the lasing mode.

Angle-resolved micro-PL spectral measurements on nanowires are useful for characterising the longitudinal modes in the nanowire. In this method, the emission pattern at the Fourier plane of the lens is imaged onto a spectrometer and spectrally resolved. A diagram of a setup is depicted in Fig. 5c. Interference fringes are observed at specific wavelengths corresponding to different amplified cavity modes (Fig. 5d). The position of these fringes depends on the nanowire length, wavelength and phase difference between the emission from the two ends. By analysing the fringe spacing and spectral position of modes, the axial order of the longitudinal modes in the nanowire can be determined [110].

An extension of the angle-resolved spectroscopy technique is Fourier plane imaging, where the emission pattern at the Fourier plane is directly imaged. This provides a 2D angle-resolved emission profile within the angular range given by the NA of the objective lens. For nanowire lasers, the Fourier plane images above threshold can show distinct features, particularly when analysed with a polariser [111]. Similar to the polarisation-resolved widefield images, matching of the Fourier plane images with simulated far-field profiles for the guided modes is required for identifying the lasing mode. The Fourier plane imaging experiments can be performed in both in side-on and end-on configurations, as shown in Fig. 5d and e. The side-on experiments are easier to perform but the Fourier plane images show interference fringes as a result of the phase-correlated emission from the two ends of the nanowire, whereas the end-on measurements are more difficult to perform but are not affected by interference and so the emission patterns are easier to simulate. Both side-on and end-on Fourier plane imaging methods require the nanowire laser to be lasing from single transverse mode, in order to unambiguously identify the lasing mode from simulations.

3. Material characterisation

Optimisation of the optoelectronic quality of the material used to fabricate lasers has long been a key challenge, as recognised since the early days of laser development by Hall [112] and Hayashi [113]. While general material quality, as determined by crystal structure, defect density and uniform doping remain important, nanowire lasers present an additional challenge due to their dimensionality and the potential for interwire disorder [59]. In this section, the measurement of key optoelectronic parameters is discussed, namely internal quantum efficiency, heterostructuring, doping and gain.

3.1. Internal quantum efficiency

The internal quantum efficiency (IQE) or photoluminescence quantum yield (PLQY) of a material is defined as the ratio of photons emitted to photons absorbed (or electron-hole pairs injected), $\nu_{\mathrm{IQE}} = \frac{\gamma_{\mathrm{out}}}{\gamma_{\mathrm{in}}}$. In conventional laser structures this value is measured either by calculation (taking into account optical effects), or more commonly by referencing the emission to a material or regime with a known quantum efficiency. In the former case, optical absorption is relatively easy to calculate given an incident optical power and a known refractive index; a calibrated integrating sphere can be used to measure the total emission [117], and best-practise approaches are now established (such as for emerging LED materials [118]). For nanowires, this approach is complicated by the difficulty in characterising the absorption of a single structure; the wavelength-scale dimensions give rise to resonances, rapidly varying absorption [119] and waveguiding [65]. Again, integrating-sphere approaches have been demonstrated by Mann [114,115], but these remain challenging experiments and variation in absorption between nanowires remains hard to characterise.

An alternative approach makes use of modelling of emission to calculate IQE. The most commonly used and simple approach involves cooling a sample to low temperature, where traps are filled and non-radiative processes can be assumed to be negligible; this is typically at cryogenic temperature where excitonic emission dominates [120,121]. By taking the ratio between emission intensity at low and high temperature, the quantum efficiency can be approximated; while this method is effective in correcting optical effects, it neglects temperature-dependant changes in refractive index or absorption. In 2015 Wang described a method to fit the power-dependant photoluminescence intensity of a single nanowire to a rate equation model [116] based on a model developed by Yoo [122]. In the high IQE limit ($\nu_{\mathrm{IQE}} > 0.5$):

$$I(P) \propto \log\left(\frac{1+n_D}{n_0}\right) - \log\left(\frac{1+n_0+n_D}{n_0}\right) + n_0, \tag{7}$$

where n_D is the doping density in normalised units of k_{NR}/B, k_{NR} is the non-radiative rate, B is the radiative recombination coefficient and n_0 is the initial carrier density. The output of this fitting is shown in Fig. 6c. This method is powerful in that it provides the IQE at a

single nanowire level, and can even be used to understand variation in emission within a single structure. However a number of assumptions are required, including the need for high IQE.

An alternative method to calculate the IQE has been demonstrated by Alanis [56], which makes use of variation in doping in inhomogeneous ensembles of nanowires. In this approach, several thousand nanowires are characterised for emission intensity and doping level. By fitting a model for IQE as a function of doping to this distribution:

$$n_{\mathrm{IQE}}(p) = \alpha \frac{Bp}{k_{\mathrm{nr}} + Bp + Cp^2}, \tag{8}$$

where α is an experimental constant, B is the radiative recombination coefficient and C is the Auger recombination coefficient, values for both α and k_{nr} can be obtained by fitting. This method has the advantage of providing statistical confidence in the measurements [59], but only effectively works in the high-doping regime [69].

3.2. Axial and radial heterostructures

A key advantage of the nanowire architecture is the flexibility provided for heterostructuring. Axial heterostructures – where properties vary along the length of the nanowire – have been explored for creating novel materials [123], nanoscale barcodes [124], electrical junctions for photovoltaics [125], and as quantum structures for lasing [126]. Radial heterostructures – where properties vary across the width of the nanowire – are used for surface passivation [100,127], strain management [73,128,129], and perhaps most importantly for quantum confinement for lasing [80,130].

The primary method for characterising heterostructures is using electron microscopy, particularly transmission electron microscopy (TEM), and scanning-TEM (STEM) as these provides direct measurements of crystallographic and atomic properties at the nanometre lengthscale [131,132]. However, for lasing the most important application of heterostructuring is quantum confinement [133]; for quantum confined structures optical techniques are well suited for characterisation.

3.2.1. Quantum confinement

By sandwiching a layer of semiconductor material between two higher bandgap materials, carriers become confined to a potential well with a thickness defined by the separation of barriers and the energy offset. In planar films, a wealth of experience exists to accurately grow quantum structures with a known thickness and composition, however, in nanowires the change of growth mechanism (for axial structures) along with effects such as shadowing make the production of uniform quantum structures challenging.

Not only can quantum structure composition vary between nanowires, it can also vary within single structures. For this reason, high-

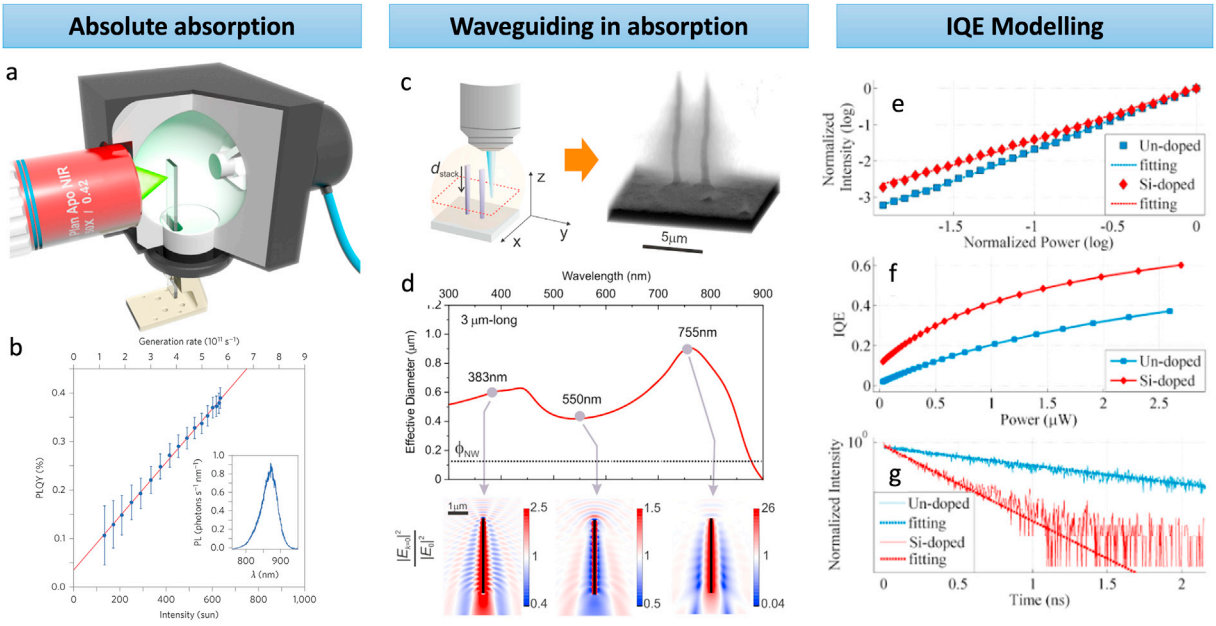

Fig. 6. Optical methods to measure optical absorption and internal quantum efficiency. Accurate calculation in the presence of geometrical anisotropy and waveguiding is challenging. (a,b) An integrating sphere provides absolute absorption and emission with appropriate calibration [114,115]. (c,d) Confocal microscopy can be used to identify and isolate waveguiding effects [65] (Reprinted with permission from ACS Photonics 2017, 4, 9, 2235–2241. Copyright 2017 American Chemical Society). (e–g) Modelling of power-dependent photoluminescence can provide an indirect measurement of internal quantum efficiency [116]. (Reprinted with permission from Nano Lett. 2015, 15, 5, 3017–3023. Copyright 2015 American Chemical Society).

through spectroscopy can provide insight into variation in quantum well width across a growth population [53,72], where the emission of the well region can be combined with modelling to infer the well thickness. Cathodoluminescence, while not purely an optical technique, is often used to characterise emission variations on the nanometre length-scale by using the electron beam of a scanning electron microscope to excite carriers [134,135] as pioneered by Gustafsson.

3.3. Doping

Doping is an extensively used technique to enhance nanowire performance by reducing the non-radiative recombination and increasing the radiative recombination rate [91,136]. The improvement of the performance is observed by an increase in the IQE of the nanowires. Optical methods are preferred to characterise doped nanowires owing to the avoidance of destructive or contact-based measurements, which are highly challenging. While Storm and colleagues demonstrated single nanowire Hall-effect measurements in 2012, this process has not often been repeated as the technical challenges in making nanoscale contacts without inducing defects is prohibitive [137]. Common optical techniques applied to study doping include Raman spectroscopy, transient terahertz photoconductivity, and photoluminescence spectroscopy [138].

Raman spectroscopy is based on inelastic light scattering where the doping concentration can be evaluated from vibrational modes. Back-scattering and forward-scattering are the most common geometries for Raman spectroscopy as illustrated in Fig. 7(a). While the forward configuration is challenging to implement, it provides access to the longitudinal optical (LO) mode for a nanowire laying on a substrate which is not observable in the back-scattering configuration [139]. While the dopant flow during growth is often well known, measuring the incorporation of dopants in the nanowires is a crucial parameter to determine doping efficiency and improve the performance [140]. The influence of incorporation and activation of the dopant is observed as broadening and red-shift of the characteristic LO mode [141]. Line shape analysis of the peak determines carrier density in the nanowire [142–144]. Ketterer and colleagues

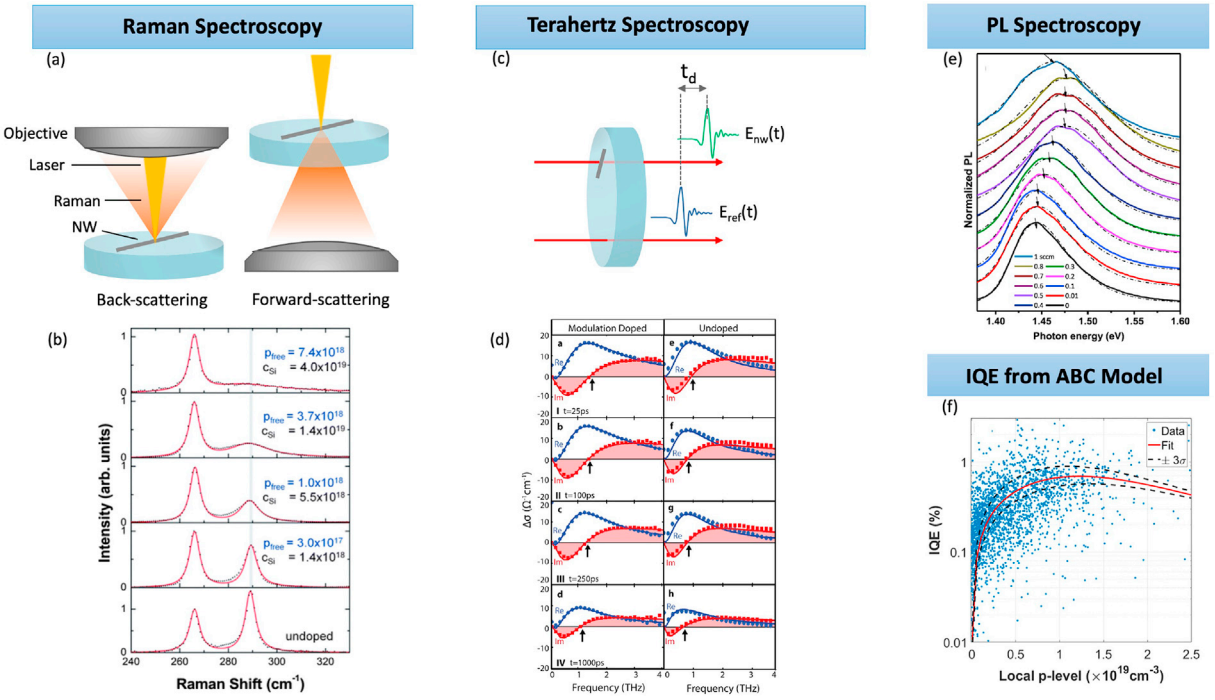

Fig. 7. (a) Raman spectroscopy configurations in back-scattering and forward-scattering. (b) Raman spectra of the LPPCM in nanowires with different free carrier concentrations in cm^{-3}. The spectra show two peaks representing the TO mode and the LO mode at around 267 cm^{-1} and 290 cm^{-1} respectively for undoped GaAs nanowires. The solid line is the fit of the data using a Lorentzian line shape for the TO phonon. c_{Si} is the nominal Si concentration and p_{free} is the free hole concentration from fitting [145]. (c) Schematic diagram of transient THz measurements on a nanowire. The change in pulse transmission as a function of time delay is converted to conductivity $\sigma(\omega)$. (d) Photoconductivity spectra obtained from OPTP for undoped and n-type Si-GaAs/AlGaAs nanowires obtained at different times after photoexcitation. The pump excitation fluence is 114 $\mu J/cm^2$ for both samples. The two components of the photoconductivity are shown in blue (real) and red (imaginary), the solid line indicates the fitted plasmon responses. Due to doping, the plasmon frequency is shifted with respect to the undoped nanowires [149]. (Reprinted with permission from Nano Lett. 2015, 15, 2, 1336–1342. Copyright 2015 American Chemical Society.) (e) Room-temperature photoluminescence spectra of n-type Si-doped GaAs nanowire arrays at different disilane flow rates. High carrier density leads to broadening and blue-shift of the peak. At very high doping level ($\sim 2 \times 10^{18}$ cm^{-3}) the peak shows red-shift and less broadening, suggesting that Si-dopant acts as acceptor (p-type) due to the amphoteric features of Si [151]. (f) IQE as a function of doping level for Zn-doped GaAs nanowires. The red line is fitting as described in a previous work [56]. The nanowire emission increases with doping followed by a decline due to Auger recombination process. (Reprinted with permission from Nano Lett. 2019, 19, 1, 362–368. Copyright 2018 American Chemical Society.)

measured the hole concentration in p-type Si-doped GaAs nanowires labelled as p_{free}, as shown in Fig. 7(b), from fitting the LO-phonon-plasmon coupled mode (LPPCM) [145]. These calculations are valid for a lower density of carriers ($<10^{19}$ cm^{-3}) as the LPPCM mode broadens and shifts to frequencies closer to mode with increasing dopant concentration in Zn-GaAs nanowires [146]. This increases the uncertainty of the line shape analysis due to overlap of the LPPCM and TO modes, as reported by Irmer and colleagues [147].

Transient terahertz (THz) photoconductivity is complementary to Raman as both probe plasmon modes that are linked to the carrier concentration [148]. This technique is based on detecting the change in the both phase and amplitude of THz pulse due to photoexcitation which can be converted to photoconductivity [149]; from this, the carrier density, mobility, and lifetimes can be extracted. There are two categories for terahertz techniques; THz-time domain spectroscopy (THz-TDS) and optical pump-THz probe spectroscopy (OPTP). THz-TDS probes carriers at equilibrium and provides the electrical conductivity $\sigma(\omega)$. OPTP is a time-resolved technique used to probe carriers at excited state and hence reveals the carrier dynamics [150]. The latter is a preferred technique due to the enhanced signal-to-noise ratio when measuring differential transmission. A sketch of this technique is shown in Fig. 7(c). Boland showed the effect of doping on the photoconductivity dynamics in n-type GaAs/AlGaAs core-shell nanowires [149] as illustrated in Fig. 7d. The plasma frequency increases with respect to the undoped material due to increased carrier density.

Photoluminescence is a common technique to study the effect of doping on nanowires – a description is given in Section 2.2. Doping results in a Fermi level shift (known as a Burstein–Moss shift) and broadening of the photoluminescence peak [91]. With appropriate calibration, the carrier concentration can then be determined using the full-width at half-maximum (FWHM) of the photoluminescence peak or the energy shift. Arab and colleagues reported a study on n-type Si-doped GaAs nanowires where such a blue-shift in photoluminescence with increased silicon incorporation was observed, as depicted in Fig. 7e [151].

Alanis studied p-type Zn-GaAs nanowires using micro-photoluminescence and calculated the active carrier concentration based on the energy-shift due to doping [56]. In this study, doping enhanced the photoluminescence emission due to an increased radiative recombination rate. This enhancement is characterised by the IQE of the nanowire which is strongly dependent on the doping density and the nanowire geometry as described in Equation (8) above. Fig. 7(f) illustrates the IQE as a function of the hole concentration for p-type GaAs nanowires [56]. At low doping levels, non-radiative recombination dominates; as doping is increased, the radiative rate increases leading to enhancement in emission. IQE declines with a further increase of doping due to the domination of Auger recombination at high doping level.

Measuring modest doping densities ($< 10^{18}$ cm^{-3}) is challenging using these techniques. For example, Burstein–Moss shift due to doping is only observed when the carrier density exceeds conduction band density of states which for InP 5×10^{17} cm^{-3} [152]. For low level doping measurements, atom probe tomography (APT) can be used [153–155] with sensitivity down to 10^{17} cm^{-3} [156].

3.4. Gain measurements

The gain, or more specifically the modal gain, provided by a nanowire is a critical parameter for laser operation. Conventional optical methods to measure gain (given in inverse length units) include variable stripe-length excitation [157] and cut-back approach (for fibre-optics), where the emission of a laser material is measured as a function of gain material length.

However both of these techniques are extremely challenging for the nanowire architecture and have their own uncertainties [157,158], due to the need for manipulation of the cavity at the micron length scale and the ease by which the end-facet reflectivity is modified by fabrication [57]. A notable exception is where pumping is spatially modified to provide a variable gain region [159]. In the earliest nanowire laser studies, the gain was estimated by comparison with thin-film gain [160], where Johnson and colleagues estimated a value of 280 cm^{-1} for ZnO nanowires. Maslov and Ning identified the challenge in these measurements; due to the strong confinement of electric fields, the modal gain in a nanowire laser can vary significantly from bulk gain in these systems [31]. More importantly, the modal gain varies strongly with mode type and with nanowire diameter [1]. It has become most common that gain calculations are performed using advanced optical simulations, such as finite-difference time-domain methods (see Section 2.1) [161]. This approach has led to the dominance of computational approaches [10,11,108].

A notable exception to the lack of experimental measurements was provided by Richters and colleagues, who used masked excitation to selectively pump specific regions of a single zinc oxide nanowire [162]. In this experiment, the modal gain was measured by comparing the emission intensity for different pump region lengths, replicating the variable stripe-length experiments previously described. The modal gain for a series of nanowires of different widths was calculated, revealing gains of up to 5000 cm^{-1}.

While direct optical measurement of the material or modal gain for a single nanowire are challenging, a closely related value – the differential gain a, where $g = a(N - N_0)$ and N and N_0 are the carrier density and transparency density – can be extracted by modelling the emission (LILO) curve as shown in Fig. 3e. Gao described the fitting of experimental light-out as a function of power-in data using a coupled rate equation model [163], where they obtained a value of 1.5×10^{-6} cm^{3}s^{-1} for GaN nanowires; in that case, the value was found to be close to the material gain as the diameter of the wires used were significantly larger than the wavelength of the laser output.

4. Cavity characterisation

A crucial component to any laser system is the cavity, which determines the lasing modes of operation. As previously discussed, the laser cavity is defined by the nanowire, and therefore the lasers can benefit from the wave-guiding effects of the nanowire, and the reflectivity of the cavity end facets. However, this means that commonly observed intra- and inter-wire geometrical variation [59] will have a large impact on the functional performance of the lasers. It is therefore important to consider the factors which affect the nanowire cavity when designing any nanowire laser.

4.1. Cavity reflectivity

The reflectivity of the cavity end facets is an important factor in determining laser performance as it governs the degree of photon-feedback within the cavity [165], as well as the extraction efficiency of the coherent light. The reflectivity is typically influenced by the nanowire refractive index, diameter [1], environment [26], facet roughness [57] and, for vapour-liquid-solid (VLS) growth, the metal catalyst [10]. It is common to investigate these effects using FDTD calculations [1,18,26,166,167], which are discussed further in section 2.1. Typically, as the nanowire radius reduces, an increasing portion of the laser mode energy is outside of the nanowire cavity: this can reduce the reflectivity when compared to the Fresnel reflection coefficients [1]. However, reduced mode confinement can also enhance the reflectivity for nanowire/substrate interfaces due to the larger reflection at the air/substrate interface [1]. It follows that the reflectivity is also strongly dependent upon the lasing cavity mode, as well as the optical polarisation, and therefore the full picture can be complex. These methods also consider idealised nanowire systems, with perfectly shaped and smooth facets: which is not the case in reality, as demonstrated by SEM images in Fig. 8a. Experimental approaches to determining the cavity reflectivity are therefore crucial to remove the ambiguity that arises from the theoretical approach.

It is challenging to directly measure the cavity reflectivity: it can be extracted by measuring parameters on which it has an effect, such as the modal gain threshold. This is approximated by equation (9) [168]:

$$g_{th} = \alpha_0 - \frac{\log(R_1 R_2)}{L} \tag{9}$$

which is influenced by changes in the end facet reflectivities R_1 and R_2, as well as the cavity length L and distributed losses α_0. More details about measuring the threshold will be provided in section 5.1.1. The cavity length can be measured either from optical or electron microscopy, luminescence microscopy [49], the mode spacing of a multi-mode nanowire laser [11] or a series of nanowire lasers [169].

Using the modal gain threshold to determine the reflectivity is problematic due to the ambiguity in the value of α_0, the physical origins of which are discussed in Section 4.2. In conventional (non-nanowire) lasers, α_0 can be measured by studying lasers of different lengths, or by optically exciting the lasing medium at different distances from the end facet [170]. The latter is a challenging approach in nanowires due to their small size, resulting in difficulties in detecting the intensity from one facet. However, the former approach is feasible, and can be highly effective as a large number of nanowire lasers can be studied. By measuring the laser threshold of a statistically significant number of nanowires, it is possible to apply correlative techniques [171] to harness the variation of cavity length and to assess how this impacts the variation of threshold with cavity length. These large datasets will allow the decoupling of α_0 and the reflectivity [2] from the data.

It can be simpler to probe the cavity reflectivity by measuring the laser coherence length L_c, which is independent of α_0. The coherence length is related to R, along with n and L by

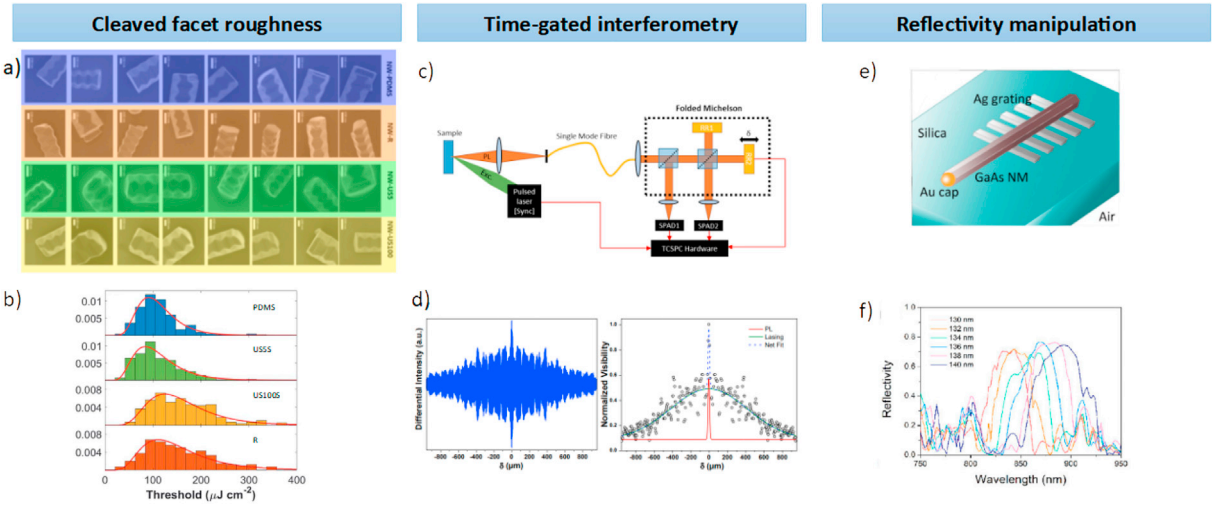

Fig. 8. A nanowire laser cavity can be characterised by imaging or spectroscopic methods. (a) SEM images showing the roughness of the cleaved facets of GaAs nanowires transferred using PDMS stamping, rubbing and ultrasound for 5 s or 100 s [57]. (b) Histograms demonstrating the impact of the transfer method on the lasing threshold of the GaAs wires: the lowest median threshold, and smoothest end facets are achieved for ultrasound for 5 s [57]. (c) An interferometric TCSPC setup capable of measuring the cavity coherence length of nanowires [49]. (d) An interferogram for the first 1 ns after excitation from a GaAsP/GaAs nanowire. A Gaussian fit to the visibility against path length difference δ is used to extract the coherence length and hence reflectivity [49]. (e) A schematic diagram for cavity length and facet reflectivity control by nanowire transfer onto a metallic grating [164]. (f) Representative shifts of the reflectivity of the metallic grating achieved by increasing the grating period [164].

$$L_c = \frac{4\pi nL}{\log\left((R_1R_2)^{-1}\right)} \tag{10}$$

where the refractive index, n, can be typically found from literature. This measurement can be achieved using an interferometer, such as the Michelson shown in Fig. 8c. By moving one of the interferometer mirrors axially, a pattern of constructive and destructive interference with distance can be observed, as in Fig. 8d. The visibility of the fringes in this interferogram is related to the coherence of the light. The coherence length can therefore be determined by fitting the variation of visibility with distance, as in Fig. 8e [49]. However, for pulsed nanowire lasers this experiment is complicated by the competing effects from stimulated and spontaneous emission. The lasing lifetime can be many times faster than spontaneous emission, and so time-gated interference techniques are required to isolate the lasing photons [172].

Another experimental approach is to measure to the Q factor, which is related to the reflectivities by equation (11):

$$Q = \frac{2\omega nL}{c\log\left((R_1R_2)^{-1}\right)}. \tag{11}$$

As discussed in section 2.2, Q can be measured using the FWHM of the PL spectrum. There is a distinction between the cavity Q factor and the lasing Q factor: the latter is higher due to a narrower FWHM of the emission peak [173]. The cavity Q can be measured using amplified spontaneous emission (ASE), whereas the lasing Q is measured from the stimulated emission spectrum. Whilst the lasing Q is often reported, it is the cavity Q which is required to determine the cavity reflectivity, provided that the cavity length is known. In nanowire lasers the Q factor can be reduced by lasing modes leaking outside of the waveguide [173] and inclined or rough sidewalls [174].

Manipulation of the cavity reflectivity is often desired: typically a higher reflectivity is required to reduce the threshold gain and enhance the performance. As previously discussed, increasing the reflectivity of the nanowire/substrate interface is easiest to achieve, as this is typically the least reflective due to the high refractive index of the substrate [1]. Transferring the nanowires onto an alternative substrate can increase this reflectivity several times [1]. However, nanowire transfer involves breaking the nanowires near the base, which is not a controlled process and can result in a rough interface with a low reflectivity, as shown in Fig. 8 (a) [57]. This can also introduce variation in the transferred nanowire length as the breakpoints will not be consistent. Various techniques exist to carry out the transfer. The simplest is by gently rubbing the as-grown nanowires onto the substrate. More involved techniques can yield improvements in the reflectivity and threshold gain: this includes solution based methods with an ultrasound bath [57] and transfer printing [175], as shown in Fig. 8 (b).

Careful nanowire design can enable controlled manipulation of the reflectivity, along with the cavity length, which can be use to select the lasing mode. This can be done in-situ for bottom-up nanowires by introducing a reflective layer, such as a distributed Bragg reflector (DBR), into the structure [176,177]. However, further development is required to reach the theoretical reflectivities of $> 90\%$. The inclusion of reflective layers in the substrate can have a similar, if reduced, effect [26]. Alternatively, top-down nanowires can be transferred onto specially designed substrates, such as a metallic grating reflector, fabricated using lithography [164], as shown in Fig. 8 (e). The reflectivity spectrum can be tuned by changing the spacing of the grating to optimise the reflection for the avelength, and lasing mode, desired.

4.2. Cavity losses

Distributed losses in the cavity, α_0, are those which scale with nanowire length, and need to be minimised to reduce the threshold gain. These effects vary depending upon the technique used to produce the nanowires.

For bottom-up techniques such as VLS [178] or selective area epitaxy [179], the growth is governed by thermodynamic processes and hence the side walls are usually defined by low free-energy crystal facets [180]. By their nature, these facets are smooth. However, sub-optimal growth conditions can lead to the formation of micro-facets [132], or a “sawtooth” pattern [181], on the sidewalls. Scattering of the optical fields from rough structures can increase the losses from the cavity [174].

Extended defects, such as dislocations, also have an impact on the modal gain. This is important for top-down nanowires, which can contain dislocations that were present in the etched epilayers [180]. In contrast, bottom-up nanowires are less susceptible due to reduced strain relaxation [182]. The defects can act as non-radiative recombination centres and so care must be taken to minimise their density.

The etching rate for top-down nanowires is anisotropic and depends on the crystal facets and the doping concentration [180]. It is possible to tune these effects to form side walls consisting of crystal facets with reduced surface states. Through careful design of the etching process, the roughness can be minimised: this has been achieved in GaN nanowires with atomic-smoothness [183].

Non-radiative recombination at surface states is another source of loss within nanowire lasers [184]. This effect can be minimised by preventing carriers from reaching these states. This surface passivation can be achieved by introducing a radial heterostructure to prevent carriers from reaching the surface [100,184,185], as discussed in Section 3. This is relatively trivial to achieve for bottom-up nanowires, but often requires transfer of wires between different reactors when applied to top-down wires. This can result in contamination of the interface and additional non-radiative recombination channels [180].

The wave-guiding properties of the nanowire can also contribute to the cavity losses. For widths similar or less than the lasing wavelength in the material, a significant proportion of the lasing energy density is outside of the side facets of the cavity and is easily lost [10,13,18]. This effect is larger for nanowires grown on their side, or which have been transferred onto a substrate, due to a reduced

refractive index difference at one of the cavity walls. Additionally, tapering of the nanowire walls can increase cavity losses [174]. These losses can be minimised by increasing the mode confinement, either by increasing the nanowire diameter, reducing the lasing wavelength or by selecting substrates with low refractive indices.

It is also important to consider the energy distribution of the lasing modes within the nanowire, and nanowire heterostructures must be designed with this in mind. For nanowires with radial quantum wells, the heterostructure is the laser gain medium, and can be aligned with the lasing mode to optimise the performance [186]. However, a poor choice of heterostructure can increase cavity losses. For examples, in AlGaAs/GaAs nanowires, photons emitted from the heterostructure will be reabsorbed by the GaAs core [53].

4.3. Geometric effects and single mode lasing

Single mode operation of nanowires can be desired for applications requiring a high spectral purity and a high communication bandwidth [187]. This can be achieved by reduction of the nanowire width or length [47], but this leads to increased cavity losses and higher threshold gains [186]. Cavity engineering can offer a promising way of achieving single mode operation without these downsides.

Often VLS-grown nanowires exhibit a tapering geometry from base to tip, which is attributed to the effect of contact angle [188] and variation in fabrication conditions, such as precursor pressure [189], temperature [180] and catalyst volume [190], throughout the growth. Tapering is also possible in wires produced by etching [180]. Whilst the tapering can increases cavity losses [174], careful design can be beneficial towards the lasing performance. The taper can reduce the number of lasing modes due to an effectively smaller diameter: this has been demonstrated in ZnO nanowires, resulting in a higher lasing intensity when compared to a uniformly thin nanowire [111].

Single mode operation is also possible by coupling two laser cavities together [46]. However, manipulating two nanowires into the required configuration is challenging due to small tolerances on the alignment and spacing required to achieve strong coupling and lasing [191]. Alternatively, focused ion beam milling can be used to cleave a single nanowire in two, which guarantees axial alignment and can precisely define the spacing and coupling strength [163].

For narrow nanowire cavities it is possible to counterbalance the increased cavity losses by careful design of the gain medium [48]. This has been demonstrated in GaAs wires, grown using selective area growth, by introducing InGaAs quantum disks and passivating the surface [186]. By performing these steps, room temperature thresholds of 48 μJ cm^{-2} were achieved with single mode operation.

5. Laser characterisation

Lasing is characterised by a number of key properties, such as narrowing of linewidth together with a marked increase in output intensity at threshold, clamping of spontaneous emission with pumping, and increase in the coherence and degree of polarisation of emission. The lasing threshold is one of the most important figure of merits, which is often reported in terms of the threshold pump power (for CW pumping) or threshold fluence (for pulsed pumping). However, the measured threshold power values are dependent on experimental conditions, such as the wavelength of the pump, beam shape and pulse width (for a pulsed pump) and so cannot be easily used for comparing performance of different devices. A more reliable metric for comparing lasers is the threshold gain or threshold carrier density, which can be estimated by fitting rate equation model to experimental data. Such analysis also provides estimates of key laser parameters such as the Q and β factor [192].

5.1. Rate equation modelling

The light-in light-out (LILO) characteristics of a laser extracted from power-dependent spectral measurements can be modelled using laser rate equations (RE). As introduced in Section 2.3.1, these are a set of coupled differential equations that describe the relationship between lasing threshold and material and cavity properties. The exact form of RE depends on the gain material, cavity and pumping method. In general for multimode lasers the RE include separate equations for each lasing mode [193], however for nanowire lasers with one or few lasing modes they are typically simplified to single mode equations. For pulsed optical pumping, the RE are typically expressed as [194]:

$$\frac{dN}{dt} = \frac{\eta}{\hbar\omega V_a} P(t) - R_{nr}(N) - R_{sp}(N) - v_g g(N) S \tag{12}$$

$$\frac{dS}{dt} = \Gamma v_g g(N) S - \frac{S}{\tau_p} + \Gamma\beta R_{sp}(N) \tag{13}$$

where the explicit dependence of radiative R_{sp} and nonradiative R_{nr} recombination rates on carrier density N can be included [192]. The pump pulse $P(t)$ can be modelled as a Gaussian function $P(t) = P_{\text{peak}} \exp[\frac{-(t-t_0)^2}{\Delta^2}]$, where P_{peak} is the pulse peak power and Δ is related to the pulse width $\Delta = \frac{\text{FWHM}}{2\sqrt{\ln 2}}$ [195]. Other parameters in the RE are: pumping efficiency η, photon energy $\hbar\omega$, active region volume V_a, cavity photon lifetime τ_p, group velocity v_g, mode confinement factor Γ and material gain $g(N)$.

Material gain generally has both a spectral and carrier density dependence, however, in RE it is usually approximated at a specific wavelength or with its peak value. The gain dependence with N is typically modelled as a linear function, as in Equation (6), which is

valid in the vicinity of the threshold and for low threshold carrier densities below gain saturation. The gain function can be derived from microscopic gain model [192] or obtained from experiments using methods discussed in Section 3.4. The latter is quite useful for new active materials for which gain coefficients or gain model is not known.

While there are several parameters in RE (photo-physical, gain and modal), reliable estimates for them can be obtained from literature, photoluminescence measurements and FDTD modelling. The two free parameters that are used for fitting the modelled LILO curve to experimental data are the cavity photon lifetime τ_p (which is related to threshold gain g_{th} and Q factor: $\frac{1}{\tau_p} = \frac{\omega}{Q} = v_g \Gamma g_{th}$) and β factor. Typically the fitting is done with normalised intensity as the total emission or power output from nanowires lasers is hard to characterise from experiments. Also, the experimental data and modelled LILO curves are plotted on a log-log scale to correctly fit the "S" shape; the parameter τ_p mostly translates the modelled curve on the horizontal axis whereas β mostly affects the shape of the 'kink' on the vertical axis.

5.1.1. Threshold estimate

The threshold carrier density N_{th} or the threshold gain $g_{th} = g(N_{th})$ estimate obtained from RE fits can be affected by the accuracy of other parameters used, in particular the gain model and pumping efficiency η. The pumping efficiency or fraction of pump power absorbed by the nanowire is highly dependent on nanowire diameter, composition, orientation and pump polarisation [196]. Reliable estimates for η can be found from 3D FDTD simulations, taking into account the geometry of the nanowire and complex refractive index of the material at the pump wavelength.

An alternative method to estimate the threshold carrier density is from the threshold gain estimate from cavity calculations [10] (using Equation (9) and reflectivity and absorption loss estimates from FDTD simulations) and then inverting the gain model $g(N)$. This approach typically underestimates the g_{th} as imperfect end-facets, tapering or other material imperfection result in a larger g_{th} for actual device.

Due to these difficulties, and the strong dependence on nanowire properties, there is a wide range of reported values of g_{th} for nanowire lasers. Passivated GaAs nanowires have values as low as 270 cm^{-1} [10,197], ZnO nanowires on silica substrates have been reported with values of 400 cm^{-1} [18] and 336 cm^{-1} has been measured for strained Ge nanowires [198]. 2D Core/shell nanowire heterostructures, such as GaAs/AlGaAs quantum wells, can reduce the threshold bulk gain of the laser [199] - however, reduction of the modal g_{th} requires high end facet reflectivities, mode confinement and good modal overlap with the gain region [130]. Optimisation of these parameters has lead to a modal g_{th} of 66.5 cm^{-1} for the HE_{31} mode in GaAs/AlGaAs nanowires on Si [199].

5.1.2. Beta factor estimate

The β factor is of great interest in laser community since a large β factor can minimise threshold [200,201]. Large β factors can be obtained by reducing cavity dimensions or by enhancing the rate of emission into lasing mode(s) [202]. Nanowire lasers typically have modest β factors of 0.01, which is because of the minimum nanowire dimensions required to obtain lasing [13,18].

As explained above, the β factor is estimated from RE fits. However, the estimates can be affected from the way data is collected and analysed, since only a fraction of the nanowire laser emission is measured in experiments and the intensity is usually normalised for fitting. For example, measuring the light emission from nanowire in end-on versus side-on configuration can give different shape LILO curves because of the angular variation of emission from nanowire end-facets and limited collection efficiency of lenses [18]. The measured spectrum from a nanowire can also vary depending on whether light is collected from nanowire ends or from in between [203]. Lastly, the measurements should cover a wide pump power range around the threshold in order to ensure that the lasing threshold is crossed and "S" shape is apparent [200]. Without this the estimates from RE fitting will be inaccurate.

5.1.3. Power output and differential quantum efficiency

The total light output and the differential quantum efficiency, which is the ratio of light output vs input pump power (above threshold), are other important figure of merits for a laser. The differential quantum efficiency can be determined from the slope of the LILO curve above threshold, when plotted with physical units on both axes (without normalisation). The LILO curve with physical units on both axes is also helpful for rate equation analysis, as discussed above. However, measuring the power emitted by nanowire lasers is challenging due to their non-directional emission and typically low power output (as this is proportional to physical size and of the order of micro watts). Also for nanowires on a substrate, majority of the light emitted may couple into the substrate instead of into free-space. Furthermore, light emission from both ends of the nanowire and non-uniform scattering from imperfect end-facets makes characterisation of total power output challenging. Some approaches are to measure the light from only one of the end-facets, as in the end-on configuration for horizontally lying nanowires [18], or measure from above for vertically integrated nanowires. In both configurations, only a fraction of total emitted light can be measured as per the collection efficiency of the measurement system. Total power emitted can be measured with an integrating sphere, but is experimentally difficult as discussed in section 3.

Given these challenges, there are various approaches that have been attempted to improve the useful power output from nanowire lasers. One approach is to fibre-couple the light from a nanowire laser by attaching nanowires to the surface of a microfibre [204–206], or by integrating nanowire lasers with passive waveguides [86,207]. Another approach is to fabricate gratings to enhance refection from one end of the nanowire and achieve one-sided light output from the low reflectivity end [164]. Gratings defined into the nanowire, or on the substrate can also modify the directionality of emission and yield vertical emission, which can help power-output characterisation [208,209]. Some further examples of out-coupling light from nanowire lasers are discussed in the following section 6.

5.2. Mode characterisation

The lasing mode(s) in nanowire lasers can be characterised using the experimental methods outlined in Section 2.4. Modelling is a necessary part of this process, for identifying potential lasing modes and validating the experimental results. Modelling requires precise measurements of the nanowire dimensions, shape and cross-sectional profile, which can be obtained from SEM and cross-sectional TEM images. Based on the structural information, FDTD or FEM simulations can be used to model the resonant modes in the nanowire cavity and calculate their respective Q factors (or threshold gain). The lasing modes are identified as those with highest Q factors (or lowest threshold gain) in the spectral region of peak material gain [192]. Numerical calculations of the supported modes also enables calculation of mode parameters, such as v_g and Γ, which are needed for the RE analysis [13]. Detailed analysis of the polarisation of mode field profiles from simulations can also help determine modal gain in nanowires with quantum confined heterostructures [130] or with anisotropic gain [31].

6. Nanowire laser integration

Contemporary research in nanowire lasers remains focused on the development of high material and cavity quality structures that can be produced on silicon for efficient coherent light emission. However, many of the promises of the nanowire laser platform require the heterointegration of single lasers onto a non-native substrate, such as for use as integrated light sources for photonic circuitry [25, 39] or for use within the biological domain [24].

6.1. Pick-and-place

The concept of picking and placing nanostructures did not begin with nanowire lasers; indeed, manipulation for carbon nanotubes was studied in the 1990s [210] and fully automated systems for silicon nanowires were reported as early as 2013 [211]. Nanowires can be manipulated into position using atomic force microscopes (AFM) [212], and Sergent and colleagues demonstrated low-threshold lasing in integrated nanowire laser-photonic crystal cavities [213,214]. While powerful for theoretical study, these approaches tend to be low-throughput; a higher-speed method applied by Strain and Hurtado makes use of transfer printing to hetero-integrate structures

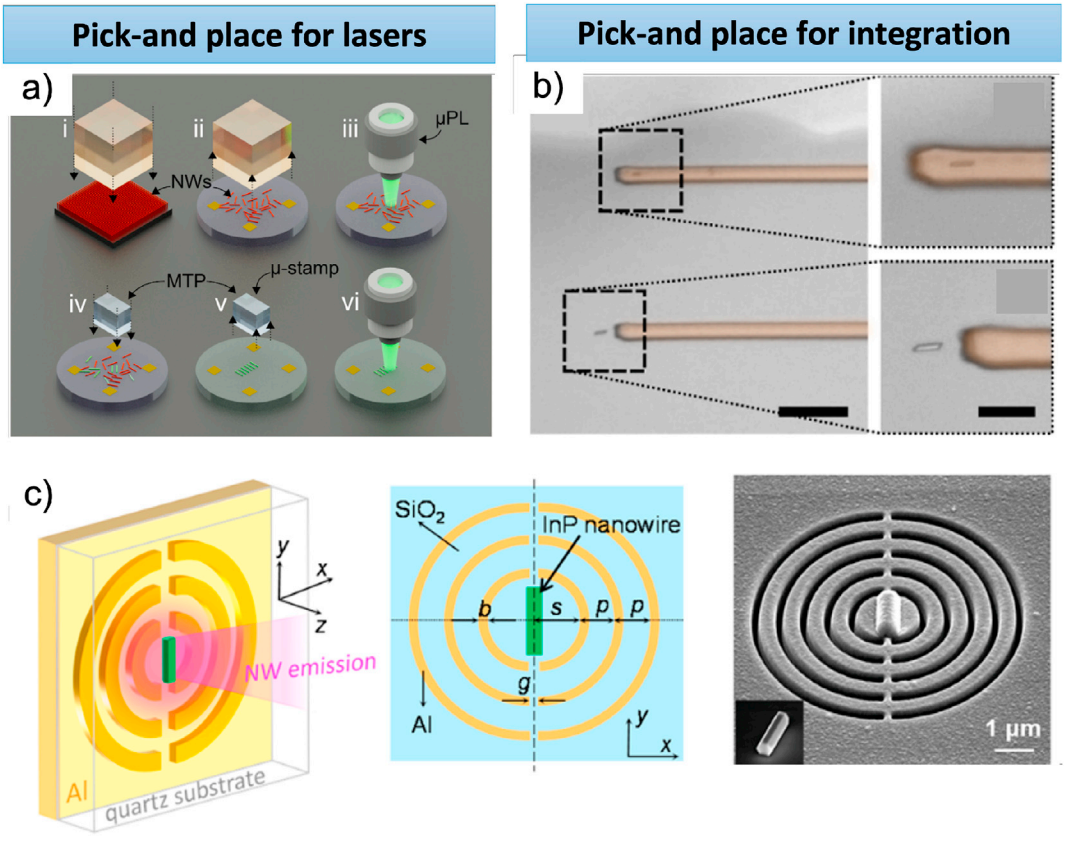

Fig. 9. Single nanowire lasers can be picked, moved and replaced. (a) A schematic of the pick and place technology for nanowire lasers [58], which can be used to place nanowire lasers onto (b) pre-fabricated optical waveguides [86] or (c) pre-fabricated antenna [208]. (Reprinted with permission from Nano Lett. 2017, 17, 10, 5990–5994 and Nano Lett. 2018, 18, 6, 3414–3420, Copyright 2017–2018 American Chemical Society.)

with high resolution and speed (see Fig. 9).

In the transfer printing methods, single nanowire lasers are first located using optical microscopy. A polymeric stamp is used to pick up and place individual lasers, by making use of differential adhesion [87,215]. This method allows for placement of single nanowires onto optical waveguides [86] or antenna structure [208], and has been used to manufacture complex multi-nanowire devices [12].

Optical characterisation of transferred structures is critical to identify any changes in threshold or lasing wavelength arising from the transfer process; Jevtics reported that transferring can impact lasing, but that a subset of transferred wires can be produced with negligible variation in figures of merit [58].

6.2. Array/coupled-cavities

Nanowire arrays and coupled cavities offer many advantages for cavity design over single nanowires, particularly for high-density vertical integration on silicon. Nanowire arrays can be engineered to support high-Q photonic resonances [216], which are not limited by the low reflectivities at nanowire/substrate interface as for single vertically standing nanowire lasers. Room temperature lasing in ordered nanowire arrays, both in 1D and 2D arrangements, have been successfully obtained [43,217,218], with devices monolithically integrated on high index substrates [219] and coupled to waveguides [28,44]. Electrical contacts have also been much easier to fabricate on nanowire arrays compared with single nanowires, with a number of successful electrically driven lasing demonstrations [47,220, 221]. Random nanowire arrays with positional disorder have also advantages of being less sensitive to structural variations in the device, and can still yield high Q modes as a result of strong scattering and interference of light in the array [47,222].

Coupled cavities of two or a few nanowires also offer advantages for mode engineering. In nanowires coupled side-by-side, the cavity can be designed with an avoided crossing to increase Q factor of one specific mode [223], and in nanowires coupled end-to-end, the cavity can selectively improve feedback for single longitudinal mode [163]. Nanowire arrays and coupled cavities offer additional design flexibility for engineering optical modes and for realising integrated nanowire lasers with small footprint and improved functionality.

7. Outlook

At the start of a third decade of research since the first reports of lasing in semiconductor nanowires, interest is primarily focusing on applications, integration, and novel materials. While the range of materials available has grown dramatically, the primary methods to study and characterise nanowire lasers has not changed. In this review, we have discussed the use of simulation, steady state and time-resolved spectroscopy, and emission imaging to determine key parameters. These parameters, spanning material quality and hetero-structuring, cavity reflectivity and losses and in-situ operando testing lie at the core of our ability to compare approaches and identify avenues of research. Given the breadth of interest in the field, it is increasingly important that measurements are comparable, and take into account differences in measurement conditions as well as unavoidable interwire inhomogeneity. While some efforts have begun to characterise and learn from wire-to-wire disorder, it is likely that future research will need to embed reproducibility at its core [59].

We note that the characterisation techniques described here are often not unique to nanowire lasers; indeed, emerging research on semiconductor rings [224], discs [225] and membranes [226] show that a range of free-standing or hetero-integrated micron-scale objects are studied. In all of these cases, optical characterisation is likely to play a key role in their development, and the methods described here are widely applicable.

Acknowledgements

PP acknowledges funding under the UKRI Future Leaders Fellowship program (MR/T021519/1).

References

[1] A.V. Maslov, C.Z. Ning, Reflection of guided modes in a semiconductor nanowire laser, Appl. Phys. Lett. 83 (6) (2003) 1237–1239, https://doi.org/10.1063/1.1599037. URL, http://aip.scitation.org/doi/10.1063/1.1599037.

[2] P. Parkinson, J.A. Alanis, S. Skalsky, Y. Zhang, H. Liu, M. Lysevych, H.H. Tan, C. Jagadish, A needle in a needlestack: exploiting functional inhomogeneity for optimized nanowire lasing, in: Proc. SPIE 11291, Quantum Dots, Nanostructures, and Quantum Materials: Growth, Characterization, and Modeling XVII, 2020, 112910K, https://doi.org/10.1117/12.2558405. URL, https://www.spiedigitallibrary.org/conference-proceedings-of-spie/11291/2558405/A-needle-in-a-needlestack-exploiting-functional-inhomogeneity-for/10.1117/12.2558405.short.

[3] N.P. Dasgupta, J. Sun, C. Liu, S. Brittman, S.C. Andrews, J. Lim, H. Gao, R. Yan, P. Yang, 25th anniversary article: semiconductor nanowires - synthesis, characterization, and applications, URL, Adv. Mater. 26 (14) (2014) 2137–2183, https://doi.org/10.1002/adma.201305929, http://www.ncbi.nlm.nih.gov/pubmed/24604701.

[4] W. Seifert, M. Borgström, K. Deppert, K.A. Dick, J. Johansson, M.W. Larsson, T. Mårtensson, N. Sköld, C. Patrik, T. Svensson, B.A. Wacaser, L. Reine Wallenberg, L. Samuelson, Growth of one-dimensional nanostructures in MOVPE, J. Cryst. Growth 272 (1–4) (2004) 211–220, https://doi.org/10.1016/j.jcrysgro.2004.09.023. URL, https://linkinghub.elsevier.com/retrieve/pii/S0022024804011169.

[5] S.D. Hersee, X. Sun, X. Wang, The controlled growth of GaN nanowires, Nano Lett. 6 (8) (2006) 1808–1811, https://doi.org/10.1021/nl060553t. URL, https://pubs.acs.org/doi/10.1021/nl060553t.

[6] N. Wang, Y. Cai, R. Zhang, Growth of nanowires, Mater. Sci. Eng. R Rep. 60 (1–6) (2008) 1–51, https://doi.org/10.1016/j.mser.2008.01.001. URL, https://linkinghub.elsevier.com/retrieve/pii/S0927796X08000028.

[7] D. Vanmaekelbergh, L.K. Van Vugt, ZnO nanowire lasers, Nanoscale 3 (7) (2011) 2783–2800, https://doi.org/10.1039/c1nr00013f. URL, http://xlink.rsc.org/?DOI=c1nr00013f.

[8] X. Duan, Y. Huang, R. Agarwal, C.M.C. Lieber, C.G. Fast, Single-nanowire electrically driven lasers, Nature 421 (6920) (2003) 241–245, https://doi.org/10.1038/nature01353. URL, http://www.nature.com/articles/nature01353.

[9] J.C. Johnson, H.-J. Choi, K.P. Knutsen, R.D. Schaller, P. Yang, R.J. Saykally, Single gallium nitride nanowire lasers, Nat. Mater. 1 (2) (2002) 106–110, https://doi.org/10.1038/nmat728. URL, http://apps.webofknowledge.com/fullhttp://www.nature.com/articles/nmat728.
[10] D. Saxena, S. Mokkapati, P. Parkinson, N. Jiang, Q. Gao, H.H. Tan, C. Jagadish, Optically pumped room-temperature GaAs nanowire lasers, Nat. Photonics 7 (12) (2013) 963–968, https://doi.org/10.1038/nphoton.2013.303. URL, http://www.nature.com/doifinder/10.1038/nphoton.2013.303, http://www.nature.com/articles/nphoton.2013.303.
[11] H. Zhu, Y. Fu, F. Meng, X. Wu, Z. Gong, Q. Ding, M.V. Gustafsson, M.T. Trinh, S. Jin, X.-Y.Y. Zhu, Lead halide perovskite nanowire lasers with low lasing thresholds and high quality factors, Nat. Mater. 14 (6) (2015) 636–642, https://doi.org/10.1038/nmat4271. URL, http://www.nature.com/doifinder/10.1038/nmat4271, http://www.nature.com/articles/nmat4271.
[12] K. Peng, D. Jevtics, F. Zhang, S. Sterzl, D.A. Damry, M.U. Rothmann, B. Guilhabert, M.J. Strain, H.H. Tan, L.M. Herz, L. Fu, M.D. Dawson, A. Hurtado, C. Jagadish, M.B. Johnston, Three-dimensional cross-nanowire networks recover full terahertz state, Science 368 (6490) (2020) 510–513, https://doi.org/10.1126/science.abb0924. URL, https://science.sciencemag.org/content/368/6490/510.
[13] C.Z. Ning, Semiconductor nanolasers, Phy. Status Solid. Basic Res. 247 (4) (2010) 774–788, https://doi.org/10.1002/pssb.200945436.
[14] C. Couteau, A. Larrue, C. Wilhelm, C. Soci, Nanowire Lasers Nanophotonics 4 (1) (2015) 90–107, https://doi.org/10.1515/nanoph-2015-0005. URL, https://www.degruyter.com/view/j/nanoph.2015.4.issue-1/nanoph-2015-0005/nanoph-2015-0005.xml.
[15] S.W. Eaton, A. Fu, A.B. Wong, C.-Z.Z. Ning, P. Yang, Semiconductor nanowire lasers, Nat. Rev. Mater. 1 (6) (2016), 16028, https://doi.org/10.1038/natrevmats.2016.28. URL, http://www.nature.com/articles/natrevmats201628.
[16] Y. Zhang, D. Saxena, M. Aagesen, H. Liu, Toward electrically driven semiconductor nanowire lasers, Nanotechnology 30 (19) (2019), 192002, https://doi.org/10.1088/1361-6528/ab000d. URL, http://stacks.iop.org/0957-4484/30/i=19/a=192002?key=crossref.7251158d04d4bddab0ec7bed09683c23.
[17] S. Arafin, X. Liu, Z. Mi, Review of recent progress of III-nitride nanowire lasers, J. Nanophotonics 7 (1) (2013), 074599, https://doi.org/10.1117/1.jnp.7.074599. URL, http://nanophotonics.spiedigitallibrary.org/article.aspx?doi=10.1117/1.JNP.7.074599.
[18] M.A. Zimmler, F. Capasso, S. Müller, C. Ronning, Optically pumped nanowire lasers: invited review, Semicond. Sci. Technol. 25 (2) (2010), 024001, https://doi.org/10.1088/0268-1242/25/2/024001. URL, http://stacks.iop.org/0268-1242/25/i=2/a=024001?key=crossref.19fed2250a6e91e6a00155a2b2f5eabe.
[19] J. Zhang, X. Yang, H. Deng, K. Qiao, U. Farooq, M. Ishaq, F. Yi, H. Liu, J. Tang, H. Song, Low-dimensional halide perovskites and their advanced optoelectronic applications, 7, http://link.springer.com/10.1007/s40820-017-0137-5, 2017. URL.
[20] H. Dong, C. Zhang, X. Liu, J. Yao, Y.S. Zhao, Materials chemistry and engineering in metal halide perovskite lasers, Chem. Soc. Rev. 49 (3) (2020) 951–982, https://doi.org/10.1039/C9CS00598F. URL, http://xlink.rsc.org/?DOI=C9CS00598F.
[21] R. Röder, C. Ronning, Review on the dynamics of semiconductor nanowire lasers, Semicond. Sci. Technol. 33 (2018), 033001, https://doi.org/10.1088/1361-6641/aaa7be. URL, http://iopscience.iop.org/article/10.1088/1361-6641/aaa7be, http://iopscience.iop.org/article/10.1088/1361-6641/aaa7be/pdf%0A, http://iopscience.iop.org/article/10.1088/1361-6641/aaa7be.
[22] G. Koblmüller, B. Mayer, T. Stettner, G. Abstreiter, J.J. Finley, GaAs-AlGaAs core-shell nanowire lasers on silicon: invited review, Semicond. Sci. Technol. 32 (5) (2017), 053001, https://doi.org/10.1088/1361-6641/aa5e45. URL, http://stacks.iop.org/0268-1242/32/i=5/a=053001?key=crossref.ba4e12afb515deb7c083b6a69d81604c.
[23] C.-Z. Ning, Semiconductor nanolasers and the size-energy-efficiency challenge: a review, Adv. Photon. 1 (2019) 1, https://doi.org/10.1117/1.AP.1.1.014002, 01, https://www.spiedigitallibrary.org/journals/advanced-photonics/volume-1/issue-01/014002/Semiconductor-nanolasers-and-the-size-energy-efficiency-challenge-a/10.1117/1.AP.1.1.014002.full. URL.
[24] X. Wu, Q. Chen, P. Xu, Y.C. Chen, B. Wu, R.M. Coleman, L. Tong, X. Fan, Nanowire lasers as intracellular probes, Nanoscale 10 (20) (2018) 9729–9735, https://doi.org/10.1039/c8nr00515j. URL, http://xlink.rsc.org/?DOI=C8NR00515J.
[25] Y. Shen, N.C. Harris, S. Skirlo, M. Prabhu, T. Baehr-Jones, M. Hochberg, X. Sun, S. Zhao, H. Larochelle, D. Englund, M. Soljačić, Deep learning with coherent nanophotonic circuits, Nat. Photonics 11 (7) (2017) 441–446, https://doi.org/10.1038/nphoton.2017.93. URL, http://arxiv.org/abs/1610.02365, http://www.nature.com/doifinder/10.1038/nphoton.2017.93, http://www.nature.com/articles/nphoton.2017.93.
[26] J. Bissinger, D. Ruhstorfer, T. Stettner, G. Koblmüller, J.J. Finley, Optimized waveguide coupling of an integrated III-V nanowire laser on silicon, J. Appl. Phys. 125 (24) (2019), 243102, https://doi.org/10.1063/1.5097405. URL, http://aip.scitation.org/doi/10.1063/1.5097405.
[27] T. Stettner, T. Kostenbader, D. Ruhstorfer, J. Bissinger, H. Riedl, M. Kaniber, G. Koblmüller, J.J. Finley, Direct coupling of coherent emission from site-selectively grown III-V nanowire lasers into proximal silicon waveguides, ACS Photonics 4 (10) (2017) 2537–2543, https://doi.org/10.1021/acsphotonics.7b00805. URL, https://pubs.acs.org/doi/10.1021/acsphotonics.7b00805.
[28] H. Kim, W.-J. Lee, T.-Y. Chang, D.L. Huffaker, Room-temperature InGaAs nanowire array band-edge lasers on patterned silicon-on-insulator platforms, Phys. Status Solidi Rapid Res. Lett. 13 (3) (2019), 1800489, https://doi.org/10.1002/pssr.201800489.
[29] S. Zhao, X. Liu, Y. Wu, Z. Mi, An electrically pumped 239 nm AlGaN nanowire laser operating at room temperature, Appl. Phys. Lett. 109 (19) (2016), 191106, https://doi.org/10.1063/1.4967180. URL, http://aip.scitation.org/doi/10.1063/1.4967180.
[30] A.V. Maslov, C.Z. Ning, Far-field emission of a semiconductor nanowire laser, Opt Lett. 29 (6) (2004) 572–574, https://doi.org/10.1364/OL.29.000572. URL, https://www.osapublishing.org/abstract.cfm?URI=ol-29-6-572, http://www.ncbi.nlm.nih.gov/pubmed/15035474.
[31] A.V. Maslov, C.Z. Ning, Modal gain in a semiconductor nanowire laser with anisotropic bandstructure, IEEE J. Quant. Electron. 40 (10) (2004) 1389–1397, https://doi.org/10.1109/JQE.2004.834767. URL, http://ieeexplore.ieee.org/document/1337019/.
[32] A.V. Maslov, C.Z. Ning, Size reduction of a semiconductor nanowire laser by using metal coating, in: M. Osinski, F. Henneberger, Y. Arakawa (Eds.), Physics and Simulation of Optoelectronic Devices XV vol. 6468, International Society for Optics and Photonics, 2007, 64680I, https://doi.org/10.1117/12.723786. URL, http://proceedings.spiedigitallibrary.org/proceeding.aspx?doi=10.1117/12.723786.
[33] F. Patolsky, G. Zheng, C.M. Lieber, Nanowire sensors for medicine and the life sciences, Nanomedicine 1 (1) (2006) 51–65, https://doi.org/10.2217/17435889.1.1.51. URL, http://www.futuremedicine.com/doi/10.2217/17435889.1.1.51.
[34] B. He, T.J. Morrow, C.D. Keating, Nanowire sensors for multiplexed detection of biomolecules, Curr. Opin. Chem. Biol. 12 (5) (2008) 522–528, https://doi.org/10.1016/j.cbpa.2008.08.027. URL, https://linkinghub.elsevier.com/retrieve/pii/S1367593108001245.
[35] Z. Wang, S. Lee, K. Koo, K. Kim, Nanowire-based sensors for biological and medical applications, IEEE Trans. NanoBioscience 15 (3) (2016) 186–199, https://doi.org/10.1109/TNB.2016.2528258. URL, http://ieeexplore.ieee.org/document/7430352/.
[36] R. Yan, J.-H. Park, Y. Choi, C.-J. Heo, S.-M. Yang, L.P. Lee, P. Yang, Nanowire-based single-cell endoscopy, Nat. Nanotechnol. 7 (3) (2012) 191–196, https://doi.org/10.1038/nnano.2011.226. URL, http://www.nature.com/articles/nnano.2011.226.
[37] R. Liu, R. Chen, A.T. Elthakeb, S.H. Lee, S. Hinckley, M.L. Khraiche, J. Scott, D. Pre, Y. Hwang, A. Tanaka, Y.G. Ro, A.K. Matsushita, X. Dai, C. Soci, S. Biesmans, A. James, J. Nogan, K.L. Jungjohann, D.V. Pete, D.B. Webb, Y. Zou, A.G. Bang, S.A. Dayeh, High density individually addressable nanowire arrays record intracellular activity from primary rodent and human stem cell derived neurons, Nano Lett. 17 (5) (2017) 2757–2764, https://doi.org/10.1021/acs.nanolett.6b04752. URL, https://pubs.acs.org/doi/10.1021/acs.nanolett.6b04752.
[38] I.A. Young, E. Mohammed, J.T. Liao, A.M. Kern, S. Palermo, B.A. Block, M.R. Reshotko, P.L. Chang, Optical I/O technology for tera-scale computing, IEEE J. Solid State Circ. 45 (1) (2010) 235–248, https://doi.org/10.1109/JSSC.2009.2034444. URL, http://ieeexplore.ieee.org/document/5357567/.
[39] C. Sun, M.T. Wade, Y. Lee, J.S. Orcutt, L. Alloatti, M.S. Georgas, A.S. Waterman, J.M. Shainline, R.R. Avizienis, S. Lin, B.R. Moss, R. Kumar, F. Pavanello, A.H. Atabaki, H.M. Cook, A.J. Ou, J.C. Leu, Y.-H. Chen, K. Asanović, R.J. Ram, M.A. Popović, V.M. Stojanović, Single-chip microprocessor that communicates directly using light, Nature 528 (7583) (2015) 534–538, https://doi.org/10.1038/nature16454. URL, http://www.nature.com/doifinder/10.1038/nature16454.
[40] B. Mayer, L. Janker, B. Loitsch, J. Treu, T. Kostenbader, S. Lichtmannecker, T. Reichert, S. Morkötter, M. Kaniber, G. Abstreiter, C. Gies, G. Koblmüller, J.J. Finley, Monolithically integrated high-β nanowire lasers on silicon, Nano Lett. 16 (1) (2016) 152–156, https://doi.org/10.1021/acs.nanolett.5b03404. URL, https://pubs.acs.org/doi/10.1021/acs.nanolett.5b03404, http://pubs.acs.org/doi/abs/10.1021/acs.nanolett.5b03404.
[41] F. Schuster, J. Kapraun, G.N. Malheiros-Silveira, S. Deshpande, C.J. Chang-Hasnain, Site-controlled growth of monolithic InGaAs/InP quantum well nanopillar lasers on silicon, Nano Lett. 17 (4) (2017) 2697–2702, https://doi.org/10.1021/acs.nanolett.7b00607. URL, http://pubs.acs.org/doi/abs/10.1021/acs.nanolett.7b00607.

[42] E.M. Fadaly, A. Dijkstra, J.R. Suckert, D. Ziss, M.A. van Tilburg, C. Mao, Y. Ren, V.T. van Lange, K. Korzun, S. Kölling, M.A. Verheijen, D. Busse, C. Rödl, J. Furthmüller, F. Bechstedt, J. Stangl, J.J. Finley, S. Botti, J.E. Haverkort, E.P. Bakkers, Direct-bandgap emission from hexagonal Ge and SiGe alloys, Nature 580 (7802) (2020) 205–209, https://doi.org/10.1038/s41586-020-2150-y. http://www.nature.com/articles/s41586-020-2150-y.
[43] H. Kim, W.J. Lee, A.C. Farrell, A. Balgarkashi, D.L. Huffaker, Telecom-wavelength bottom-up nanobeam lasers on silicon-on-insulator, Nano Lett. 17 (9) (2017) 5244–5250, https://doi.org/10.1021/acs.nanolett.7b01360. URL, https://pubs.acs.org/doi/10.1021/acs.nanolett.7b01360.
[44] H. Kim, T.Y. Chang, W.J. Lee, D.L. Huffaker, III-V nanowire array telecom lasers on (001) silicon-on-insulator photonic platforms, Appl. Phys. Lett. 115 (2019), 213101, https://doi.org/10.1063/1.5126721. URL, https://aip.scitation.org/doi/10.1063/1.5126721.
[45] A. Yokoo, M. Takiguchi, M.D. Birowosuto, K. Tateno, G. Zhang, E. Kuramochi, A. Shinya, H. Taniyama, M. Notomi, Subwavelength nanowire lasers on a silicon photonic crystal operating at telecom wavelengths, ACS Photonics 4 (2) (2017) 355–362, https://doi.org/10.1021/acsphotonics.6b00830. URL, https://pubs.acs.org/doi/10.1021/acsphotonics.6b00830.
[46] W.T. Tsang, N.A. Olsson, R.A. Logan, High-speed direct single-frequency modulation with large tuning rate and frequency excursion in cleaved-coupled-cavity semiconductor lasers, Appl. Phys. Lett. 42 (8) (1983) 650–652, https://doi.org/10.1063/1.94053. URL, http://aip.scitation.org/doi/10.1063/1.94053.
[47] N. Li, K. Liu, V.J. Sorger, D.K. Sadana, Monolithic III–V on silicon plasmonic nanolaser structure for optical interconnects, Sci. Rep. 5 (1) (2015), 14067, https://doi.org/10.1038/srep14067. http://www.nature.com/articles/srep14067.
[48] D. Ren, L. Ahtapodov, J.S. Nilsen, J. Yang, A. Gustafsson, J. Huh, G.J. Conibeer, A.T. Van Helvoort, B.O. Fimland, H. Weman, Single-mode near-infrared lasing in a GaAsSb-based nanowire superlattice at room temperature, Nano Lett. 18 (4) (2018) 2304–2310, https://doi.org/10.1021/acs.nanolett.7b05015. URL, https://pubs.acs.org/doi/10.1021/acs.nanolett.7b05015.
[49] S. Skalsky, Y. Zhang, J.A. Alanis, H.A. Fonseka, A.M. Sanchez, H. Liu, P. Parkinson, Heterostructure and Q-factor engineering for low-threshold and persistent nanowire lasing, Light Sci. Appl. 9 (1) (2020) 43, https://doi.org/10.1038/s41377-020-0279-y. URL, http://www.nature.com/articles/s41377-020-0279-y.
[50] A. Thurn, J. Bissinger, S. Meinecke, P. Schmiedeke, S. S. Oh, W. W. Chow, K. Lüdge, G. Koblmüller, J. J. Finley, Self-induced ultrafast electron-hole plasma temperature oscillations in nanowire lasers, arXiv. URL http://arxiv.org/abs/2108.11784.
[51] T.J. Evans, A. Schlaus, Y. Fu, X. Zhong, T.L. Atallah, M.S. Spencer, L.E. Brus, S. Jin, X.Y. Zhu, Continuous-wave lasing in cesium lead bromide perovskite nanowires, Adv. Opt. Mater. 6 (2) (2018), 1700982, https://doi.org/10.1002/adom.201700982.
[52] J. Ho, J. Tatebayashi, S. Sergent, C.F. Fong, S. Iwamoto, Y. Arakawa, Low-threshold near-infrared GaAs-AlGaAs core-shell nanowire plasmon laser, ACS Photonics 2 (1) (2015) 165–171, https://doi.org/10.1021/ph5003945. URL, http://pubs.acs.org/doi/abs/10.1021/ph5003945.
[53] J.A. Alanis, D. Saxena, S. Mokkapati, N. Jiang, K. Peng, X. Tang, L. Fu, H.H. Tan, C. Jagadish, P. Parkinson, Large-scale statistics for threshold optimization of optically pumped nanowire lasers, Nano Lett. 17 (8) (2017) 4860–4865, https://doi.org/10.1021/acs.nanolett.7b01725. URL, http://pubs.acs.org/doi/abs/10.1021/acs.nanolett.7b01725, http://pubs.acs.org/doi/10.1021/acs.nanolett.7b01725.
[54] M. Zapf, C. Ronning, R. Röder, High temperature limit of semiconductor nanowire lasers, Appl. Phys. Lett. 110 (17) (2017), 173103, https://doi.org/10.1063/1.4982629. URL, http://aip.scitation.org/doi/10.1063/1.4982629.
[55] Y. Fu, H. Zhu, A.W. Schrader, D. Liang, Q. Ding, P. Joshi, L. Hwang, X.Y. Zhu, S. Jin, Nanowire lasers of formamidinium lead halide perovskites and their stabilized alloys with improved stability, Nano Lett. 16 (2) (2016) 1000–1008, https://doi.org/10.1021/acs.nanolett.5b04053. URL, https://pubs.acs.org/doi/10.1021/acs.nanolett.5b04053.
[56] J.A. Alanis, M. Lysevych, T. Burgess, D. Saxena, S. Mokkapati, S. Skalsky, X. Tang, P. Mitchell, A.S. Walton, H.H. Tan, C. Jagadish, P. Parkinson, Optical study of p-doping in GaAs nanowires for low-threshold and high-yield lasing, Nano Lett. 19 (1) (2019) 362–368, https://doi.org/10.1021/acs.nanolett.8b04048. URL, http://pubs.acs.org/doi/10.1021/acs.nanolett.8b04048.
[57] J.A. Alanis, Q. Chen, M. Lysevych, T. Burgess, L. Li, Z. Liu, H.H. Tan, C. Jagadish, P. Parkinson, Threshold reduction and yield improvement of semiconductor nanowire lasers: via processing-related end-facet optimization, Nanoscale Adv. 1 (11) (2019) 4393–4397, https://doi.org/10.1039/c9na00479c. URL, http://xlink.rsc.org/?DOI=C9NA00479C.
[58] D. Jevtics, J. McPhillimy, B. Guilhabert, J.A. Alanis, H.H. Tan, C. Jagadish, M.D. Dawson, A. Hurtado, P. Parkinson, M.J. Strain, Characterization, selection, and microassembly of nanowire laser systems, Nano Lett. 20 (3) (2020) 1862–1868, https://doi.org/10.1021/acs.nanolett.9b05078. URL, https://pubs.acs.org/doi/10.1021/acs.nanolett.9b05078.
[59] R. Al-Abri, H. Choi, P. Parkinson, Measuring, controlling and exploiting heterogeneity in optoelectronic nanowires, J. Phys.: Photonics 3 (2) (2021), 022004, https://doi.org/10.1088/2515-7647/abe282. URL, https://iopscience.iop.org/article/10.1088/2515-7647/abe282.
[60] J. Arturo Alanis, M. Lysevych, T. Burgess, D. Saxena, S. Mokkapati, S. Skalsky, X. Tang, P. Mitchell, A.S. Walton, H. Hoe Tan, C. Jagadish, P. Parkinson, J.A. Alanis, M. Lysevych, T. Burgess, D. Saxena, S. Mokkapati, S. Skalsky, X. Tang, P. Mitchell, A.S. Walton, H.H. Tan, C. Jagadish, P. Parkinson, Optical study of p-doping in GaAs nanowires for low-threshold and high-yield lasing, Nano Lett. 19 (1) (2018) 362–368, https://doi.org/10.1021/acs.nanolett.8b04048. URL, http://pubs.acs.org/doi/10.1021/acs.nanolett.8b04048.
[61] R. Paniagua-Domínguez, G. Grzela, J.G. Rivas, J.A. Sánchez-Gil, Enhanced and directional emission of semiconductor nanowires tailored through leaky/guided modes, Nanoscale 5 (21) (2013) 10582–10590, https://doi.org/10.1039/C3NR03001F.
[62] G. Bulgarini, D. Dalacu, P.J. Poole, J. Lapointe, M.E. Reimer, V. Zwiller, Far field emission profile of pure wurtzite InP nanowires, Appl. Phys. Lett. 105 (19) (2014), 191113, https://doi.org/10.1063/1.4901437.
[63] B. Gallinet, J. Butet, O.J.F. Martin, Numerical methods for nanophotonics: standard problems and future challenges, Laser Photon. Rev. 9 (6) (2015) 577–603, https://doi.org/10.1002/lpor.201500122.
[64] S. Mokkapati, D. Saxena, H.H. Tan, C. Jagadish, Semiconductor nanowire optoelectronic devices, in: Semiconductors and Semimetals vol. 94, Academic Press Inc., 2016, pp. 1–15, https://doi.org/10.1016/bs.semsem.2015.07.007.
[65] R. Frederiksen, G. Tutuncuoglu, F. Matteini, K.L. Martinez, A. Fontcuberta i Morral, E. Alarcon-Llado, Visual understanding of light absorption and waveguiding in standing nanowires with 3D fluorescence confocal microscopy, ACS Photonics 4 (9) (2017) 2235–2241, https://doi.org/10.1021/acsphotonics.7b00434. URL, https://pubs.acs.org/doi/10.1021/acsphotonics.7b00434.
[66] J. Xing, X.F. Liu, Q. Zhang, S.T. Ha, Y.W. Yuan, C. Shen, T.C. Sum, Q. Xiong, Vapor phase synthesis of organometal halide perovskite nanowires for tunable room-temperature nanolasers, Nano Lett. 15 (7) (2015) 4571–4577, https://doi.org/10.1021/acs.nanolett.5b01166. URL, https://pubs.acs.org/doi/10.1021/acs.nanolett.5b01166.
[67] S.A. Lyon, Spectroscopy of hot carriers in semiconductors, J. Lumin. 35 (3) (1986) 121–154, https://doi.org/10.1016/0022-2313(86)90066-9.
[68] F. Urbach, The long-wavelength edge of photographic sensitivity and of the electronic absorption of solids, Phys. Rev. 92 (5) (1953), https://doi.org/10.1103/PhysRev.92.1324, 1324–1324, https://link.aps.org/doi/10.1103/PhysRev.92.1324. URL.
[69] G. Borghs, K. Bhattacharyya, K. Deneffe, P. Van Mieghem, R. Mertens, Band-gap narrowing in highly doped n- and p-type GaAs studied by photoluminescence spectroscopy, J. Appl. Phys. 66 (9) (1989) 4381–4386, https://doi.org/10.1063/1.343958. URL, http://aip.scitation.org/doi/10.1063/1.343958.
[70] H.J. Joyce, Q. Gao, H.H. Tan, C. Jagadish, Y. Kim, M.A. Fickenscher, S. Perera, T.B. Hoang, L.M. Smith, H.E. Jackson, J.M. Yarrison-Rice, X. Zhang, J. Zou, High purity GaAs nanowires free of planar defects: growth and characterization, Adv. Funct. Mater. 18 (23) (2008) 3794–3800, https://doi.org/10.1002/adfm.200800625. URL, https://onlinelibrary.wiley.com/doi/10.1002/adfm.200800625.
[71] R.C. Miller, D.A. Kleinman, Excitons in GaAs quantum wells, J. Lumin. 30 (1–4) (1985) 520–540, https://doi.org/10.1016/0022-2313(85)90075-4. URL, https://www.sciencedirect.com/science/article/pii/0022231385900754.
[72] C.L. Davies, P. Parkinson, N. Jiang, J.L. Boland, S. Conesa-Boj, H.H. Tan, C. Jagadish, L.M. Herz, M.B. Johnston, Low ensemble disorder in quantum well tube nanowires, Nanoscale 7 (48) (2015) 20531–20538, https://doi.org/10.1039/C5NR06996C. URL, http://xlink.rsc.org/?DOI=C5NR06996C.
[73] L. Balaghi, G. Bussone, R. Grifone, R. Hübner, J. Grenzer, M. Ghorbani-Asl, A.V. Krasheninnikov, H. Schneider, M. Helm, E. Dimakis, Widely tunable GaAs bandgap via strain engineering in core/shell nanowires with large lattice mismatch, Nat. Commun. 10 (1) (2019) 2793, https://doi.org/10.1038/s41467-019-10654-7. URL, http://www.nature.com/articles/s41467-019-10654-7.
[74] P. Wurfel, The chemical potential of radiation, J. Phys. C Solid State Phys. 15 (18) (1982) 3967–3985, https://doi.org/10.1088/0022-3719/15/18/012.

[75] G. Lasher, F. Stern, Spontaneous and stimulated recombination radiation in semiconductors, Phys. Rev. 133 (2A) (1964) A553–A563, https://doi.org/10.1103/PhysRev.133.A553. URL, https://link.aps.org/doi/10.1103/PhysRev.133.A553.

[76] I. Pelant, J. Valenta, Luminescence Spectroscopy of Semiconductors, Oxford University Press, 2012. URL, https://www.google.co.uk/books/edition/Luminescence_Spectroscopy_of_Semiconduct/w3MtuntlIFAC?hl=en&gbpv=1&dq=%E2%80%A2%E2%80%9CLuminescence+spectroscopy+of+semiconductors&pg=PP1&printsec=frontcover.

[77] M. Ledinsky, T. Schönfeldová, J. Holovský, E. Aydin, Z. Hájková, L. Landová, N. Neyková, A. Fejfar, S. De Wolf, Temperature dependence of the Urbach energy in lead iodide perovskites, J. Phys. Chem. Lett. 10 (6) (2019) 1368–1373, https://doi.org/10.1021/acs.jpclett.9b00138. URL, https://pubs.acs.org/doi/10.1021/acs.jpclett.9b00138.

[78] H. Kroemer, A proposed class of hetero-junction injection lasers, Proc. IEEE 51 (12) (1963) 1782–1783, https://doi.org/10.1109/PROC.1963.2706. URL, http://ieeexplore.ieee.org/document/1444636/.

[79] Z.I. Alferov, Nobel Lecture: the double heterostructure concept and its applications in physics, electronics, and technology, Rev. Mod. Phys. 73 (3) (2001) 767–782, https://doi.org/10.1103/RevModPhys.73.767. URL, https://link.aps.org/doi/10.1103/RevModPhys.73.767.

[80] F. Qian, Y. Li, S. Gradečak, H.-G.G. Park, Y. Dong, Y. Ding, Z.L. Wang, C.M. Lieber, Multi-quantum-well nanowire heterostructures for wavelength-controlled lasers, Nat. Mater. 7 (9) (2008) 701–706, https://doi.org/10.1038/nmat2253. URL, http://www.nature.com/articles/nmat2253, http://www.nature.com/doifinder/10.1038/nmat2253.

[81] M. Montazeri, H.E. Jackson, L.M. Smith, J.M. Yarrison-Rice, J.-H. Kang, Q. Gao, H.H. Tan, C. Jagadish, Transient Rayleigh scattering: a new probe of picosecond carrier dynamics in a single semiconductor nanowire, Nano Lett. 12 (10) (2012) 5389–5395, https://doi.org/10.1021/nl302767u. URL, http://pubs.acs.org/doi/10.1021/nl302767u.

[82] P. Parkinson, J. Lloyd-Hughes, Q. Gao, H.H. Tan, C. Jagadish, M.B. Johnston, L.M. Herz, Transient terahertz conductivity of GaAs nanowires, Nano Lett. 7 (7) (2007) 2162–2165, https://doi.org/10.1021/nl071162x. URL, https://pubs.acs.org/doi/10.1021/nl071162x.

[83] C.K. Yong, J. Wong-Leung, H.J. Joyce, J. Lloyd-Hughes, Q. Gao, H.H. Tan, C. Jagadish, M.B. Johnston, L.M. Herz, Direct observation of charge-carrier heating at WZ-ZB InP nanowire heterojunctions, Nano Lett. 13 (9) (2013) 4280–4287, https://doi.org/10.1021/nl402050q. URL, https://pubs.acs.org/doi/10.1021/nl402050q.

[84] L.W. Casperson, Threshold characteristics of multimode laser oscillators, J. Appl. Phys. 46 (12) (1975) 5194–5201, https://doi.org/10.1063/1.321311. URL, http://aip.scitation.org/doi/10.1063/1.321311.

[85] R. Röder, D. Ploss, A. Kriesch, R. Buschlinger, S. Geburt, U. Peschel, C. Ronning, Polarization features of optically pumped CdS nanowire lasers, J. Phys. Appl. Phys. 47 (39) (2014), 394012, https://doi.org/10.1088/0022-3727/47/39/394012. URL, https://iopscience.iop.org/article/10.1088/0022-3727/47/39/394012.

[86] D. Jevtics, A. Hurtado, B. Guilhabert, J. McPhillimy, G. Cantarella, Q. Gao, H.H. Tan, C. Jagadish, M.J. Strain, M.D. Dawson, Integration of semiconductor nanowire lasers with polymeric waveguide devices on a mechanically flexible substrate, Nano Lett. 17 (10) (2017) 5990–5994, https://doi.org/10.1021/acs.nanolett.7b02178. URL, https://pubs.acs.org/doi/10.1021/acs.nanolett.7b02178.

[87] B. Guilhabert, A. Hurtado, D. Jevtics, Q. Gao, H.H. Tan, C. Jagadish, M.D. Dawson, Transfer printing of semiconductor nanowires with lasing emission for controllable nanophotonic device fabrication, ACS Nano 10 (4) (2016) 3951–3958, https://doi.org/10.1021/acsnano.5b07752. URL, https://pubs.acs.org/doi/10.1021/acsnano.5b07752.

[88] A. Pan, W. Zhou, E.S.P. Leong, R. Liu, A.H. Chin, B. Zou, C.Z. Ning, Continuous alloy-composition spatial grading and superbroad wavelength-tunable nanowire lasers on a single chip, Nano Lett. 9 (2) (2009) 784–788, https://doi.org/10.1021/n1803456k. URL, https://pubs.acs.org/doi/10.1021/nl803456k.

[89] G. Aman, F. Mohammadi, M. Fränzl, M. Lysevych, H.H. Tan, C. Jagadish, H. Schmitzer, M. Cahay, H.P. Wagner, Effect of Au substrate and coating on the lasing characteristics of GaAs nanowires, Sci. Rep. 2021 11 (1) (2021) 1–9, https://doi.org/10.1038/s41598-021-00855-w, 1 11, https://www.nature.com/articles/s41598-021-00855-w. URL.

[90] S. H. Pan, Q. Gu, A. E. Amili, F. Vallini, Y. Fainman, Dynamic hysteresis in a coherent high-β nanolaser, Optica, Vol. 3, Issue 11, pp. 1260-1265 3 (11) (2016) 1260–1265. doi:10.1364/OPTICA.3.001260. URL https://www.osapublishing.org/viewmedia.cfm?uri=optica-3-11-1260&seq=0&html=true https://www.osapublishing.org/abstract.cfm?uri=optica-3-11-1260 https://www.osapublishing.org/optica/abstract.cfm?uri=optica-3-11-1260.

[91] H.C. Casey, F. Stern, Concentration-dependent absorption and spontaneous emission of heavily doped GaAs, J. Appl. Phys. 47 (2) (1976) 631–643, https://doi.org/10.1063/1.322626. URL, http://aip.scitation.org/doi/10.1063/1.322626.

[92] H.J. Joyce, C.J. Docherty, Q. Gao, H.H. Tan, C. Jagadish, J. Lloyd-Hughes, L.M. Herz, M.B. Johnston, Electronic properties of GaAs, InAs and InP nanowires studied by terahertz spectroscopy, Nanotechnology 24 (21) (2013), 214006, https://doi.org/10.1088/0957-4484/24/21/214006. URL http://stacks.iop.org/0957-4484/24/i=21/a=214006?key=crossref.3ddd730e84f137f4d4de09739ab00ec8, https://iopscience.iop.org/article/10.1088/0957-4484/24/21/214006.

[93] M.A. Zimmler, J. Bao, F. Capasso, S. Müller, C. Ronning, Laser action in nanowires: observation of the transition from amplified spontaneous emission to laser oscillation, Appl. Phys. Lett. 93 (5) (2008), 051101, https://doi.org/10.1063/1.2965797. URL, http://aip.scitation.org/doi/10.1063/1.2965797.

[94] R. Röder, T.P.H. Sidiropoulos, C. Tessarek, S. Christiansen, R.F. Oulton, C. Ronning, Ultrafast dynamics of lasing semiconductor nanowires, Nano Lett. 15 (7) (2015) 4637–4643, https://doi.org/10.1021/acs.nanolett.5b01271. URL, http://pubs.acs.org/doi/10.1021/acs.nanolett.5b01271.

[95] A.P. Schlaus, M.S. Spencer, K. Miyata, F. Liu, X. Wang, I. Datta, M. Lipson, A. Pan, X.Y. Zhu, How lasing happens in CsPbBr 3 perovskite nanowires, Nat. Commun. 10 (1) (2019) 265, https://doi.org/10.1038/s41467-018-07972-7. URL, http://www.nature.com/articles/s41467-018-07972-7.

[96] L. Wittenbecher, E. Viñas Boström, J. Vogelsang, S. Lehman, K.A. Dick, C. Verdozzi, D. Zigmantas, A. Mikkelsen, Unraveling the ultrafast hot electron dynamics in semiconductor nanowires, ACS Nano 15 (1) (2021) 1133–1144, https://doi.org/10.1021/acsnano.0c08101.

[97] C.Q. Xia, M. Monti, J.L. Boland, L.M. Herz, J. Lloyd-Hughes, M.R. Filip, M.B. Johnston, Hot electron cooling in InSb probed by ultrafast time-resolved terahertz cyclotron resonance, Phys. Rev. B 103 (24) (2021), 245205, https://doi.org/10.1103/PhysRevB.103.245205. URL, https://journals.aps.org/prb/abstract/10.1103/PhysRevB.103.245205.

[98] H.P. Wagner, M. Kaveh, Q. Gao, H. Tan, C. Jagadish, W. Langbein, Population dynamics and dephasing of excitons and electron-hole pairs in polytype wurtzite/zinc-blende InP nanowires, Phys. Rev. B 95 (4) (2017), 045305, https://doi.org/10.1103/PhysRevB.95.045305. URL, https://journals.aps.org/prb/abstract/10.1103/PhysRevB.95.045305.

[99] C. Gutsche, R. Niepelt, M. Gnauck, A. Lysov, W. Prost, C. Ronning, F.-J. Tegude, Direct determination of minority carrier diffusion lengths at axial GaAs nanowire p–n junctions, Nano Lett. 12 (3) (2012) 1453–1458, https://doi.org/10.1021/NL204126N. URL, https://pubs.acs.org/doi/abs/10.1021/nl204126n.

[100] P. Parkinson, H.J. Joyce, Q. Gao, H.H. Tan, X. Zhang, J. Zou, C. Jagadish, L.M. Herz, M.B. Johnston, Carrier lifetime and mobility enhancement in nearly defect-free core-shell nanowires measured using time-resolved terahertz spectroscopy, Nano Lett. 9 (9) (2009) 3349–3353, https://doi.org/10.1021/nl9016336. URL, http://pubs.acs.org/doi/abs/10.1021/nl9016336.

[101] H. Yokoyama, S.D. Brorson, Rate equation analysis of microcavity lasers, J. Appl. Phys. 66 (10) (1989) 4801–4805, https://doi.org/10.1063/1.343793. URL, http://aip.scitation.org/doi/10.1063/1.343793.

[102] G. Bjork, Y. Yamamoto, Analysis of semiconductor microcavity lasers using rate equations, IEEE J. Quant. Electron. 27 (11) (1991) 2386–2396, https://doi.org/10.1109/3.100877. URL, http://ieeexplore.ieee.org/document/100877/.

[103] C.Y. Yang, C.T. Chia, H.Y. Chen, S. Gwo, K.H. Lin, Ultrafast carrier dynamics in GaN nanorods, Appl. Phys. Lett. 105 (21) (2014), 212105, https://doi.org/10.1063/1.4902927. URL, https://aip.scitation.org/doi/abs/10.1063/1.4902927.

[104] T. Burgess, D. Saxena, S. Mokkapati, Z. Li, C.R. Hall, J.A. Davis, Y. Wang, L.M. Smith, L. Fu, P. Caroff, H.H. Tan, C. Jagadish, Doping-enhanced radiative efficiency enables lasing in unpassivated GaAs nanowires, Nat. Commun. 7 (May) (2016), 11927, https://doi.org/10.1038/ncomms11927. URL http://www.nature.com/doifinder/10.1038/ncomms11927.

[105] X.-X. Zhang, C. Würth, L. Zhao, U. Resch-Genger, N.P. Ernsting, M. Sajadi, Femtosecond broadband fluorescence upconversion spectroscopy: improved setup and photometric correction, Rev. Sci. Instrum. 82 (6) (2011), 063108, https://doi.org/10.1063/1.3597674. URL, https://aip.scitation.org/doi/abs/10.1063/1.3597674.

[106] B. Schmidt, S. Laimgruber, W. Zinth, P. Gilch, A broadband Kerr shutter for femtosecond fluorescence spectroscopy, Appl. Phys. B 76 (8) (2003) 809–814, https://doi.org/10.1007/s00340-003-1230-7. URL, http://link.springer.com/10.1007/s00340-003-1230-7.

[107] S.T. Cundiff, Coherent spectroscopy of semiconductors, Opt Express 16 (Issue 7) (2008) 4639–4664, https://doi.org/10.1364/OE.16.004639, 16 (7), https://www.osapublishing.org/viewmedia.cfm?uri=oe-16-7-4639&seq=0&html=true, https://www.osapublishing.org/abstract.cfm?uri=oe-16-7-4639, https://www.osapublishing.org/oe/abstract.cfm?uri=oe-16-7-4639. URL.

[108] D. Saxena, F. Wang, Q. Gao, S. Mokkapati, H.H. Tan, C. Jagadish, Mode profiling of semiconductor nanowire lasers, Nano Lett. 15 (8) (2015) 5342–5348, https://doi.org/10.1021/acs.nanolett.5b01713. URL, https://pubs.acs.org/doi/10.1021/acs.nanolett.5b01713.

[109] L.K. van Vugt, S. Rühle, D. Vanmaekelbergh, Phase-correlated nondirectional laser emission from the end facets of a ZnO nanowire, Nano Lett. 6 (12) (2006) 2707–2711, https://doi.org/10.1021/nl0616227.

[110] L. Sun, M.L. Ren, W. Liu, R. Agarwal, Resolving parity and order of fabry-pérot modes in semiconductor nanostructure waveguides and lasers: youngs interference experiment revisited, Nano Lett. 14 (11) (2014) 6564–6571, https://doi.org/10.1021/nl503176w. URL, https://pubs.acs.org/doi/10.1021/nl503176w.

[111] R. Röder, T.P. Sidiropoulos, R. Buschlinger, M. Riediger, U. Peschel, R.F. Oulton, C. Ronning, Mode switching and filtering in nanowire lasers, Nano Lett. 16 (4) (2016) 2878–2884, https://doi.org/10.1021/acs.nanolett.6b00811. URL, https://pubs.acs.org/doi/10.1021/acs.nanolett.6b00811.

[112] R.N. Hall, G.E. Fenner, J.D. Kingsley, T.J. Soltys, R.O. Carlson, Coherent light emission from GaAs junctions, Phys. Rev. Lett. 9 (9) (1962) 366–368, https://doi.org/10.1103/PhysRevLett.9.366. URL, https://link.aps.org/doi/10.1103/PhysRevLett.9.366.

[113] I. Hayashi, M.B. Panish, P.W. Foy, S. Sumski, Junction lasers which operate continuously at room temperature, Appl. Phys. Lett. 17 (3) (1970) 109–111, https://doi.org/10.1063/1.1653326. URL, http://aip.scitation.org/doi/10.1063/1.1653326.

[114] S.A. Mann, S.Z. Oener, A. Cavalli, J.E.M. Haverkort, E.P.A.M. Bakkers, E.C. Garnett, Quantifying losses and thermodynamic limits in nanophotonic solar cells, Nat. Nanotechnol. 11 (12) (2016) 1071–1075, https://doi.org/10.1038/nnano.2016.162. URL, http://www.nature.com/articles/nnano.2016.162.

[115] S.A. Mann, B. Sciacca, Y. Zhang, J. Wang, E. Kontoleta, H. Liu, E.C. Garnett, Integrating sphere microscopy for direct absorption measurements of single nanostructures, ACS Nano 11 (2) (2017) 1412–1418, https://doi.org/10.1021/acsnano.6b06534. URL, https://pubs.acs.org/doi/10.1021/acsnano.6b06534.

[116] F. Wang, Q. Gao, K. Peng, Z. Li, Z. Li, Y. Guo, L. Fu, L.M. Smith, H.H. Tan, C. Jagadish, Spatially resolved doping concentration and nonradiative lifetime profiles in single Si-doped InP nanowires using photoluminescence mapping, Nano Lett. 15 (5) (2015) 3017–3023, https://doi.org/10.1021/nl504929n. URL, https://pubs.acs.org/doi/10.1021/nl504929n.

[117] S. Leyre, E. Coutino-Gonzalez, J.J. Joos, J. Ryckaert, Y. Meuret, D. Poelman, P.F. Smet, G. Durinck, J. Hofkens, G. Deconinck, P. Hanselaer, Absolute determination of photoluminescence quantum efficiency using an integrating sphere setup, Rev. Sci. Instrum. 85 (12) (2014), 123115, https://doi.org/10.1063/1.4903852. URL, https://aip.scitation.org/doi/abs/10.1063/1.4903852.

[118] M. Anaya, B.P. Rand, R.J. Holmes, D. Credgington, H.J. Bolink, R.H. Friend, J. Wang, N.C. Greenham, S.D. Stranks, Best practices for measuring emerging light-emitting diode technologies, Nat. Photonics 13 (12) (2019) 818–821, https://doi.org/10.1038/s41566-019-0543-y, 12 13, https://www.nature.com/articles/s41566-019-0543-y. URL.

[119] Y. Chen, N. Anttu, S. Sivakumar, E. Gompou, M. H. Magnusson, Optical far-field extinction of a single GaAs nanowire towards in situ size control of aerotaxy nanowire growth, Nanotechnology 31 (13). doi:10.1088/1361-6528/ab5fe4.

[120] S. Watanabe, N. Yamada, M. Nagashima, Y. Ueki, C. Sasaki, Y. Yamada, T. Taguchi, K. Tadatomo, H. Okagawa, H. Kudo, Internal quantum efficiency of highly-efficient In_\{x\}Ga_\{1-x\}N-based near-ultraviolet light-emitting diodes, Appl. Phys. Lett. 83 (24) (2003) 4906–4908, https://doi.org/10.1063/1.1633672. URL, http://aip.scitation.org/doi/10.1063/1.1633672.

[121] L.V. Titova, T.B. Hoang, H.E. Jackson, L.M. Smith, J.M. Yarrison-Rice, Y. Kim, H.J. Joyce, H.H. Tan, C. Jagadish, Temperature dependence of photoluminescence from single core-shell GaAs-AlGaAs nanowires, Appl. Phys. Lett. 89 (17) (2006), 173126, https://doi.org/10.1063/1.2364885. URL, http://aip.scitation.org/doi/10.1063/1.2364885.

[122] Y.-S. Yoo, T.-M. Roh, J.-H. Na, S.J. Son, Y.-H. Cho, Simple analysis method for determining internal quantum efficiency and relative recombination ratios in light emitting diodes, Appl. Phys. Lett. 102 (21) (2013), 211107, https://doi.org/10.1063/1.4807485. URL, http://aip.scitation.org/doi/10.1063/1.4807485.

[123] C.Y. Wen, M.C. Reuter, J. Bruley, J. Tersoff, S. Kodambaka, E.A. Stach, F.M. Ross, Formation of compositionally abrupt axial heterojunctions in silicon-germanium nanowires, Science 326 (5957) (2009) 1247–1250, https://doi.org/10.1126/science.1178606. URL, http://www.ncbi.nlm.nih.gov/pubmed/19965471.

[124] J. Oracz, K. Adolfsson, V. Westphal, C. Radzewicz, M.T. Borgström, S.J. Sahl, C.N. Prinz, S.W. Hell, Ground state depletion nanoscopy resolves semiconductor nanowire barcode segments at room temperature, Nano Lett. 17 (4) (2017) 2652–2659, https://doi.org/10.1021/ACS.NANOLETT.7B00468. URL, https://pubs.acs.org/doi/full/10.1021/acs.nanolett.7b00468.

[125] E. Barrigón, O. Hultin, D. Lindgren, F. Yadegari, M.H. Magnusson, L. Samuelson, L.I. Johansson, M.T. Björk, GaAs nanowire pn-junctions produced by low-cost and high-throughput aerotaxy, Nano Lett. 18 (2) (2018) 1088–1092, https://doi.org/10.1021/acs.nanolett.7b04609.

[126] G. Zhang, M. Takiguchi, K. Tateno, T. Tawara, M. Notomi, H. Gotoh, Telecom-band lasing in single InP/InAs heterostructure nanowires at room temperature, Sci. Adv. 5 (2) (2019), eaat8896, https://doi.org/10.1126/sciadv.aat8896. URL, https://advances.sciencemag.org/lookup/doi/10.1126/sciadv.aat8896, http://advances.sciencemag.org/content/5/2/eaat8896?rss=1.

[127] S. Perera, M.A. Fickenscher, H.E. Jackson, L.M. Smith, J.M. Yarrison-Rice, H.J. Joyce, Q. Gao, H.H. Tan, C. Jagadish, X. Zhang, J. Zou, Nearly intrinsic exciton lifetimes in single twin-free GaAsAlGaAs core-shell nanowire heterostructures, Appl. Phys. Lett. 93 (5) (2008), 053110, https://doi.org/10.1063/1.2967877. URL, http://scitation.aip.org/content/aip/journal/apl/93/5/10.1063/1.2967877.

[128] A. Kar, Q. Li, P.C. Upadhya, M. Ah Seo, J. Wright, T.S. Luk, G.T. Wang, R.P. Prasankumar, The influence of radial heterostructuring on carrier dynamics in gallium nitride nanowires, Appl. Phys. Lett. 101 (14) (2012), 143104, https://doi.org/10.1063/1.4756915. URL, http://aip.scitation.org/doi/10.1063/1.4756915.

[129] Y. Zhang, G. Davis, H.A. Fonseka, A. Velichko, A. Gustafsson, T. Godde, D. Saxena, M. Aagesen, P.W. Parkinson, J.A. Gott, S. Huo, A.M. Sanchez, D.J. Mowbray, H. Liu, Highly strained III-V-V coaxial nanowire quantum wells with strong carrier confinement, ACS Nano 13 (5) (2019) 5931–5938, https://doi.org/10.1021/acsnano.9b01775. URL, http://pubs.acs.org/doi/10.1021/acsnano.9b01775.

[130] D. Saxena, N. Jiang, X. Yuan, S. Mokkapati, Y. Guo, H.H. Tan, C. Jagadish, Design and room-temperature operation of GaAs/AlGaAs multiple quantum well nanowire lasers, Nano Lett. 16 (8) (2016) 5080–5086, https://doi.org/10.1021/acs.nanolett.6b01973. URL, http://pubs.acs.org/doi/abs/10.1021/acs.nanolett.6b01973, https://pubs.acs.org/doi/10.1021/acs.nanolett.6b01973.

[131] N. Jiang, Q. Gao, P. Parkinson, J. Wong-Leung, S. Mokkapati, S. Breuer, H.H. Tan, C.L. Zheng, J. Etheridge, C. Jagadish, Enhanced minority carrier lifetimes in GaAs/AlGaAs core-shell nanowires through shell growth optimization, Nano Lett. 13 (11) (2013) 5135–5140, https://doi.org/10.1021/nl4023385.

[132] H.A. Fonseka, A.V. Velichko, Y. Zhang, J.A. Gott, G.D. Davis, R. Beanland, H. Liu, D.J. Mowbray, A.M. Sanchez, Self-formed quantum wires and dots in GaAsP–GaAsP core–shell nanowires, Nano Lett. 19 (6) (2019) 4158–4165, https://doi.org/10.1021/acs.nanolett.9b01673. URL, http://pubs.acs.org/doi/10.1021/acs.nanolett.9b01673.

[133] N. Holonyak, R.M. Kolbas, R.D. Dupuis, P.D. Dapkus, Quantum-well heterostructure lasers, IEEE J. Quant. Electron. 16 (2) (1980) 170–186, https://doi.org/10.1109/JQE.1980.1070447. URL, http://ieeexplore.ieee.org/document/1070447/.

[134] J. Bolinsson, M. Ek, J. Trägårdh, K. Mergenthaler, D. Jacobsson, M.E. Pistol, L. Samuelson, A. Gustafsson, GaAs/AlGaAs heterostructure nanowires studied by cathodoluminescence, Nano Res. 7 (4) (2014) 1–18, https://doi.org/10.1007/s12274-014-0414-2.

[135] A. Gustafsson, N. Jiang, C. Zheng, J. Etheridge, Q. Gao, H.H. Tan, C. Jagadish, J. Wong-Leung, Cathodoluminescence visualisation of local thickness variations of GaAs/AlGaAs quantum-well tubes on nanowires, Nanotechnology 31 (42) (2020), 424001, https://doi.org/10.1088/1361-6528/ab9fb3. URL, https://iopscience.iop.org/article/10.1088/1361-6528/ab9fb3.

[136] M.K. Hudait, P. Modak, K.S. Rao, S.B. Krupanidhi, Low temperature photoluminescence properties of Zn-doped GaAs, Mater. Sci. Eng. B 57 (1) (1998) 62–70, https://doi.org/10.1016/s0921-5107(98)00259-1.

[137] K. Storm, F. Halvardsson, M. Heurlin, D. Lindgren, A. Gustafsson, P.M. Wu, B. Monemar, L. Samuelson, Spatially resolved Hall effect measurement in a single semiconductor nanowire, Nat. Nanotechnol. 7 (11) (2012) 718–722, https://doi.org/10.1038/nnano.2012.190. URL, http://www.nature.com/doifinder/10.1038/nnano.2012.190.

[138] W. Kim, L. Güniat, A. Fontcuberta I Morral, V. Piazza, Doping Challenges and Pathways to Industrial Scalability of III-V Nanowire Arrays, 2021, p. 3, https://doi.org/10.1063/5.0031549.

[139] F. Amaduzzi, E. Alarcón-Lladó, H. Hautmann, R. Tanta, F. Matteini, G. Tütüncüolu, T. Vosch, J. Nygård, T. Jespersen, E. Uccelli, A. Fontcuberta I Morral, Tuning the response of non-allowed Raman modes in GaAs nanowires, J. Phys. Appl. Phys. 49 (9). doi:10.1088/0022-3727/49/9/095103.

[140] S. Devkota, M. Parakh, S. Johnson, P. Ramaswamy, M. Lowe, A. Penn, L. Reynolds, S. Iyer, A study of n-doping in self-catalyzed GaAsSb nanowires using GaTe dopant source and ensemble nanowire near-infrared photodetector, Nanotechnology 31 (50). doi:10.1088/1361-6528/abb506.

[141] S.K. Ojha, P.K. Kasanaboina, C. Lewis Reynolds, T.A. Rawdanowicz, Y. Liu, R.M. White, S. Iyer, Incorporation of Be dopant in GaAs core and core–shell nanowires by molecular beam epitaxy, J. Vac. Sci. Technol. B Nanotechnol. Microelectron.: Mater. Process. Meas. Phenom. 34 (2) (2016), 02L114, https://doi.org/10.1116/1.4943600.

[142] H. Potts, M. Friedl, F. Amaduzzi, K. Tang, G. Tütüncüoglu, F. Matteini, E. Alarcon Lladó, P.C. McIntyre, A. Fontcuberta I Morral, From twinning to pure zincblende catalyst-free InAs(Sb) nanowires, Nano Lett. 16 (1) (2016) 637–643, https://doi.org/10.1021/acs.nanolett.5b04367.

[143] K. Jeganathan, R. K. Debnath, R. Meijers, T. Stoica, R. Calarco, D. Grützmacher, H. Lüth, Raman scattering of phonon-plasmon coupled modes in self-assembled GaN nanowires, J. Appl. Phys. 105 (12). doi:10.1063/1.3148862.

[144] P. Tchoulfian, F. Donatini, F. Levy, B. Amstatt, A. Dussaigne, P. Ferret, E. Bustarret, J. Pernot, Thermoelectric and micro-Raman measurements of carrier density and mobility in heavily Si-doped GaN wires, Appl. Phys. Lett. 103 (20) (2013) 1–5, https://doi.org/10.1063/1.4829857.

[145] B. Ketterer, E. Mikheev, E. Uccelli, A. Fontcuberta I Morral, Compensation mechanism in silicon-doped gallium arsenide nanowires, Appl. Phys. Lett. 97 (22). doi:10.1063/1.3517254.

[146] M. Rizzo Piton, E. Koivusalo, T. Hakkarainen, H. V. A. Galeti, A. De Giovanni Rodrigues, S. Talmila, S. Souto, D. Lupo, Y. Galvão Gobato, M. Guina, Gradients of Be-dopant concentration in self-catalyzed GaAs nanowires, Nanotechnology 30 (33). doi:10.1088/1361-6528/ab1a97.

[147] G. Irmer, M. Wenzel, J. Monecke, Light scattering by a multicomponent plasma coupled with longitudinal-optical phonons: Raman spectra of p-type GaAs:Zn, Phys. Rev. B 56 (15) (1997) 9524–9538, https://doi.org/10.1103/PhysRevB.56.9524.

[148] J.L. Boland, F. Amaduzzi, S. Sterzl, H. Potts, L.M. Herz, A. Fontcuberta I Morral, M.B. Johnston, High electron mobility and insights into temperature-dependent scattering mechanisms in InAsSb nanowires, Nano Lett. 18 (6) (2018) 3703–3710, https://doi.org/10.1021/acs.nanolett.8b00842.

[149] J.L. Boland, S. Conesa-Boj, P. Parkinson, G. Tütüncüoglu, F. Matteini, D. Rüffer, A. Casadei, F. Amaduzzi, F. Jabeen, C.L. Davies, H.J. Joyce, L.M. Herz, A. Fontcuberta I Morral, M.B. Johnston, Modulation doping of GaAs/AlGaAs core-shell nanowires with effective defect passivation and high electron mobility, Nano Lett. 15 (2) (2015) 1336–1342, https://doi.org/10.1021/nl504566t.

[150] H. J. Joyce, J. L. Boland, C. L. Davies, S. A. Baig, M. B. Johnston, A review of the electrical properties of semiconductor nanowires: insights gained from terahertz conductivity spectroscopy, Semicond. Sci. Technol. 31 (10). doi:10.1088/0268-1242/31/10/103003.

[151] S. Arab, M. Yao, C. Zhou, P. Daniel Dapkus, S.B. Cronin, Doping concentration dependence of the photoluminescence spectra of *n* -type GaAs nanowires, Appl. Phys. Lett. 108 (18) (2016), 182106, https://doi.org/10.1063/1.4947504. URL, http://aip.scitation.org/doi/10.1063/1.4947504.

[152] C. Liu, L. Dai, L. P. You, W. J. Xu, G. G. Qin, Blueshift of electroluminescence from single n-InP nanowire/p-Si heterojunctions due to the Burstein-Moss effect, Nanotechnology 19 (46). doi:10.1088/0957-4484/19/46/465203.

[153] J. Qu, W. Choi, P. Katal Mohseni, X. Li, Y. Zhang, H. Chen, S. Ringer, R. Zheng, Direct observation of dopants distribution and diffusion in GaAs planar nanowires with atom probe tomography, ACS Appl. Mater. Interfaces 8 (39) (2016) 26244–26250, https://doi.org/10.1021/acsami.6b08919.

[154] Z. Sun, O. Hazut, B.C. Huang, Y.P. Chiu, C.S. Chang, R. Yerushalmi, L.J. Lauhon, D.N. Seidman, Dopant diffusion and activation in silicon nanowires fabricated by ex situ doping: a correlative study via atom-probe tomography and scanning tunneling spectroscopy, Nano Lett. 16 (7) (2016) 4490–4500, https://doi.org/10.1021/acs.nanolett.6b01693.

[155] J.R. Riley, R.A. Bernal, Q. Li, H.D. Espinosa, G.T. Wang, L.J. Lauhon, Atom probe tomography of a-axis GaN nanowires: analysis of nonstoichiometric evaporation behavior, ACS Nano 6 (5) (2012) 3898–3906, https://doi.org/10.1021/nn2050517.

[156] S. Zhang, E.R. Hemesath, D.E. Perea, E. Wijaya, J.L. Lensch-Falk, L.J. Lauhon, Relative influence of surface states and bulk impurities on the electrical properties of ge nanowires, Nano Lett. 9 (9) (2009) 3268–3274, https://doi.org/10.1021/nl901548u.

[157] L. Dal Negro, P. Bettotti, M. Cazzanelli, D. Pacifici, L. Pavesi, Applicability conditions and experimental analysis of the variable stripe length method for gain measurements, Opt Commun. 229 (1–6) (2004) 337–348, https://doi.org/10.1016/J.OPTCOM.2003.10.051.

[158] L. Cerdán, Variable Stripe Length method: influence of stripe length choice on measured optical gain, Opt Lett. 42 (Issue 24) (2017) 5258–5261, https://doi.org/10.1364/OL.42.005258, 42 (24), https://www.osapublishing.org/viewmedia.cfm?uri=ol-42-24-5258&seq=0&html=true, https://www.osapublishing.org/abstract.cfm?uri=ol-42-24-5258, https://www.osapublishing.org/ol/abstract.cfm?uri=ol-42-24-5258. URL.

[159] J. Li, C. Meng, Y. Liu, X. Wu, Y. Lu, Y. Ye, L. Dai, L. Tong, X. Liu, Q. Yang, Wavelength tunable CdSe nanowire lasers based on the absorption-emission-absorption process, Adv. Mater. 25 (6) (2013) 833–837, https://doi.org/10.1002/adma.201203692.

[160] J.C. Johnson, H. Yan, R.D. Schaller, L.H. Haber, R.J. Saykally, P. Yang, Single nanowire lasers, J. Phys. Chem. B 105 (46) (2001) 11387–11390, https://doi.org/10.1021/jp012304t. URL, https://pubs.acs.org/doi/10.1021/jp012304t.

[161] S. Wang, Z. Hu, H. Yu, W. Fang, M. Qiu, L. Tong, Endface reflectivities of optical nanowires, Opt Express 17 (13) (2009), 10881, https://doi.org/10.1364/OE.17.010881. URL, http://www.ncbi.nlm.nih.gov/pubmed/19550488https://www.osapublishing.org/oe/abstract.cfm?uri=oe-17-13-10881.

[162] J.P. Richters, J. Kalden, M. Gnauck, C. Ronning, C.P. Dietrich, H. von Wenckstern, M. Grundmann, J. Gutowski, T. Voss, Modal gain and its diameter dependence in single-ZnO micro- and nanowires, Semicond. Sci. Technol. 27 (1) (2011), 015005, https://doi.org/10.1088/0268-1242/27/1/015005.

[163] H. Gao, A. Fu, S.C. Andrews, P. Yang, Cleaved-coupled nanowire lasers, Proc. Natl. Acad. Sci. U.S.A. 110 (3) (2013) 865–869, https://doi.org/10.1073/pnas.1217335110. URL, http://www.ncbi.nlm.nih.gov/pubmed/23284173, http://www.pubmedcentral.nih.gov/articlerender.fcgi?artid=PMC3549097.

[164] W. Wei, X. Yan, X. Zhang, Miniaturized GaAs nanowire laser with a metal grating reflector, Nanomaterials 10 (4) (2020) 680, https://doi.org/10.3390/nano10040680. URL, https://www.mdpi.com/2079-4991/10/4/680.

[165] Z. Yu, Y. Wu, L. Xiao, J. Chen, Q. Liao, J. Yao, H. Fu, Organic phosphorescence nanowire lasers, J. Am. Chem. Soc. 139 (18) (2017) 6376–6381, https://doi.org/10.1021/jacs.7b01574. URL, https://pubs.acs.org/doi/10.1021/jacs.7b01574.

[166] B. Mayer, L. Janker, D. Rudolph, B. Loitsch, T. Kostenbader, G. Abstreiter, G. Koblmüller, J.J. Finley, Continuous wave lasing from individual GaAs-AlGaAs core-shell nanowires, Appl. Phys. Lett. 108 (7) (2016), 071107, https://doi.org/10.1063/1.4942506. URL, http://scitation.aip.org/content/aip/journal/apl/108/7/10.1063/1.4942506.

[167] S. Chen, M. Jansson, J.E. Stehr, Y. Huang, F. Ishikawa, W.M. Chen, I.A. Buyanova, Dilute nitride nanowire lasers based on a GaAs/GaNAs core/shell structure, Nano Lett. 17 (3) (2017) 1775–1781, https://doi.org/10.1021/acs.nanolett.6b05097. URL, http://pubs.acs.org/doi/abs/10.1021/acs.nanolett.6b05097.

[168] T. Nobis, M. Grundmann, Low-order optical whispering-gallery modes in hexagonal nanocavities, Phy. Rev. A Atom. Mol. Opt. Phy. 72 (6) (2005) 1–11, https://doi.org/10.1103/PhysRevA.72.063806.

[169] P. Parkinson, J.A. Alanis, K. Peng, D. Saxena, S. Mokkapati, N. Jiang, L. Fu, H.H. Tan, C. Jagadish, Modal refractive index measurement in nanowire lasers—a correlative approach, Nano Futures 2 (3) (2018), 035004, https://doi.org/10.1088/2399-1984/aad0c6. URL, http://iopscience.iop.org/article/10.1088/2399-1984/aad0c6, http://stacks.iop.org/2399-1984/2/i=3/a=035004?key=crossref.228ddf78af0e38c7d6c720f99506fe5d, https://iopscience.iop.org/article/10.1088/2399-1984/aad0c6.

[170] M.D. McGehee, R. Gupta, S. Veenstra, E.K. Miller, M.A. Díaz-García, A.J. Heeger, Amplified spontaneous emission from photopumped films of a conjugated polymer, Phys. Rev. B 58 (11) (1998) 7035–7039, https://doi.org/10.1103/PhysRevB.58.7035. URL, https://link.aps.org/doi/10.1103/PhysRevB.58.7035.

[171] B. Sun, M. Fernandez, A.S. Barnard, Statistics, damned statistics and nanoscience – using data science to meet the challenge of nanomaterial complexity, Nanoscale Horiz. 1 (2) (2016) 89–95, https://doi.org/10.1039/C5NH00126A. URL, http://xlink.rsc.org/?DOI=C5NH00126A.

[172] Y. Liu, H. Fang, A. Rasmita, Y. Zhou, J. Li, T. Yu, Q. Xiong, N. Zheludev, J. Liu, W. Gao, Room temperature nanocavity laser with interlayer excitons in 2D heterostructures, Sci. Adv. 5 (2019), eaav4506.
[173] K. Ding, C.Z. Ning, Metallic subwavelength-cavity semiconductor nanolasers, Light Sci. Appl. 1 (7) (2012), https://doi.org/10.1038/lsa.2012.20 e20–e20, http://www.nature.com/articles/lsa201220. URL.
[174] M. Marell, Gap Plasmon Mode Distributed Feedback Lasers, Ph.D. thesis, TU/e, Eindhoven, 2011, p. 6, https://doi.org/10.6100/IR712629.
[175] C.H. Lee, D.R. Kim, X. Zheng, Fabricating nanowire devices on diverse substrates by simple transfer-printing methods, Proc. Natl. Acad. Sci. U.S.A. 107 (22) (2010) 9950–9955, https://doi.org/10.1073/pnas.0914031107.
[176] J. Tatebayashi, S. Kako, J. Ho, Y. Ota, S. Iwamoto, Y. Arakawa, Growth of InGaAs/GaAs nanowire-quantum dots on AlGaAs/GaAs distributed Bragg reflectors for laser applications, J. Cryst. Growth 468 (2017) 144–148, https://doi.org/10.1016/j.jcrysgro.2016.12.022. URL, https://linkinghub.elsevier.com/retrieve/pii/S0022024816308818.
[177] X. Zhang, H. Yang, Y. Zhang, H. Liu, Design of high-quality reflectors for vertical nanowire lasers on Si, arXiv (2021), 2103.16922. URL, https://arxiv.org/abs/2103.16922v1.
[178] E.I. Givargizov, Fundamental aspects of VLS growth, J. Cryst. Growth 31 (C) (1975) 20–30, https://doi.org/10.1016/0022-0248(75)90105-0. URL, https://www.sciencedirect.com/science/article/pii/0022024875901050.
[179] J. Motohisa, J. Noborisaka, J. Takeda, M. Inari, T. Fukui, Catalyst-free selective-area MOVPE of semiconductor nanowires on (111)B oriented substrates, J. Cryst. Growth 272 (1–4) (2004) 180–185, https://doi.org/10.1016/j.jcrysgro.2004.08.118. URL, https://linkinghub.elsevier.com/retrieve/pii/S0022024804010899.
[180] P. McIntyre, A. Fontcuberta i Morral, Semiconductor nanowires: to grow or not to grow? Mater. Today Nano 9 (2020), 100058 https://doi.org/10.1016/j.mtnano.2019.100058. URL, https://www.sciencedirect.com/science/article/pii/S2588842019301270?viahttps://linkinghub.elsevier.com/retrieve/pii/S2588842019301270.
[181] F.M. Ross, J. Tersoff, M.C. Reuter, Sawtooth faceting in silicon nanowires, Phys. Rev. Lett. 95 (14) (2005), 146104, https://doi.org/10.1103/PhysRevLett.95.146104. URL, https://link.aps.org/doi/10.1103/PhysRevLett.95.146104.
[182] K. L. Kavanagh, Misfit dislocations in nanowire heterostructures, Semicond. Sci. Technol. 25 (2). doi:10.1088/0268-1242/25/2/024006.
[183] M. Behzadirad, M. Nami, N. Wostbrock, M.R. Zamani Kouhpanji, D.F. Feezell, S.R.J. Brueck, T. Busani, Scalable top-down approach tailored by interferometric lithography to achieve large-area single-mode GaN nanowire laser arrays on sapphire substrate, ACS Nano 12 (3) (2018) 2373–2380, https://doi.org/10.1021/acsnano.7b07653. URL, https://pubs.acs.org/doi/10.1021/acsnano.7b07653.
[184] D. Rudolph, S. Funk, M. Döblinger, S. Morkötter, S. Hertenberger, L. Schweickert, J. Becker, S. Matich, M. Bichler, D. Spirkoska, I. Zardo, J.J. Finley, G. Abstreiter, G. Koblmüller, Spontaneous alloy composition ordering in GaAs-AlGaAs core-shell nanowires, Nano Lett. 13 (4) (2013) 1522–1527, https://doi.org/10.1021/nl3046816. URL, http://pubs.acs.org/doi/10.1021/nl3046816.
[185] C. Himwas, S. Collin, P. Rale, N. Chauvin, G. Patriarche, F. Oehler, F.H. Julien, L. Travers, J.-C. Harmand, M. Tchernycheva, In situ passivation of GaAsP nanowires, Nanotechnology 28 (49) (2017), 495707, https://doi.org/10.1088/1361-6528/aa9533. URL, https://iopscience.iop.org/article/10.1088/1361-6528/aa9533.
[186] X. Zhang, R. Yi, N. Gagrani, Z. Li, F. Zhang, X. Gan, X. Yao, X. Yuan, N. Wang, J. Zhao, P. Chen, W. Lu, L. Fu, H.H. Tan, C. Jagadish, Ultralow threshold, single-mode InGaAs/GaAs multiquantum disk nanowire lasers, ACS Nano (2021), https://doi.org/10.1021/acsnano.1c02425 acsnano.1c02425, https://pubs.acs.org/doi/10.1021/acsnano.1c02425. URL.
[187] C. Zhang, C.-L. Zou, H. Dong, Y. Yan, J. Yao, Y.S. Zhao, Dual-color single-mode lasing in axially coupled organic nanowire resonators, Sci. Adv. 3 (7) (2017), e1700225, https://doi.org/10.1126/sciadv.1700225. URL, https://advances.sciencemag.org/lookup/doi/10.1126/sciadv.1700225.
[188] V.G. Dubrovskii, Refinement of nucleation theory for vapor–liquid–solid nanowires, Cryst. Growth Des. 17 (5) (2017) 2589–2593, https://doi.org/10.1021/acs.cgd.7b00124. URL, https://pubs.acs.org/doi/10.1021/acs.cgd.7b00124.
[189] D. Jacobsson, F. Panciera, J. Tersoff, M.C. Reuter, S. Lehmann, S. Hofmann, K.A. Dick, F.M. Ross, Interface dynamics and crystal phase switching in GaAs nanowires, Nature 531 (7594) (2016) 317–322, https://doi.org/10.1038/nature17148. URL, http://www.nature.com/articles/nature17148.
[190] J. Tang, J.-L. Maurice, W. Chen, S. Misra, M. Foldyna, E.V. Johnson, P. Roca i Cabarrocas, Plasma-assisted growth of silicon nanowires by Sn catalyst: step-by-step observation, Nanoscale Res. Lett. 11 (1) (2016) 455, https://doi.org/10.1186/s11671-016-1681-5. URL, http://nanoscalereslett.springeropen.com/articles/10.1186/s11671-016-1681-5.
[191] Y. Xiao, C. Meng, P. Wang, Y. Ye, H. Yu, S. Wang, F. Gu, L. Dai, L. Tong, Single-nanowire single-mode laser, Nano Lett. 11 (3) (2011) 1122–1126, https://doi.org/10.1021/nl1040308. URL, https://pubs.acs.org/doi/10.1021/nl1040308.
[192] L.A. Coldren, S.W. Corzine, M.L. Mašanović, Diode Lasers and Photonic Integrated Circuits, second ed., Wiley, Hoboken, NJ, USA, 2012 https://doi.org/10.1002/9781118148167.
[193] S.-W. Chang, T.-R. Lin, S.L. Chuang, Theory of plasmonic fabry-perot nanolasers, Opt Express 18 (14) (2010) 15039–15053, https://doi.org/10.1364/OE.18.015039. URL, http://www.ncbi.nlm.nih.gov/pubmed/20639990.
[194] S.W. Eaton, M. Lai, N.A. Gibson, A.B. Wong, L. Dou, J. Ma, L.-W.W. Wang, S.R. Leone, P. Yang, Lasing in robust cesium lead halide perovskite nanowires, Proc. Natl. Acad. Sci. USA 113 (8) (2016) 1993–1998, https://doi.org/10.1073/pnas.1600789113. URL, http://www.pnas.org/lookup/doi/10.1073/pnas.1600789113.
[195] S.H. Pan, S.S. Deka, A. El Amili, Q. Gu, Y. Fainman, Nanolasers: second-order intensity correlation, direct modulation and electromagnetic isolation in array architectures, Prog. Quant. Electron. 59 (May) (2018) 1–18, https://doi.org/10.1016/j.pquantelec.2018.05.001. URL, https://doi.org/10.1016/j.pquantelec.2018.05.001.
[196] J. Wang, Highly polarized photoluminescence and photodetection from single indium phosphide nanowires, Science 293 (5534) (2001) 1455–1457, https://doi.org/10.1126/science.1062340. URL, http://www.sciencemag.org/cgi/doi/10.1126/science.1062340.
[197] Z. Azimi, N. Gagrani, J. Qu, O. L. C. Lem, S. Mokkapati, J. M. Cairney, R. Zheng, H. H. Tan, C. Jagadish, J. Wong-Leung, Understanding the role of facets and twin defects in the optical performance of GaAs nanowires for laser applications, Nanoscale Horiz.:10.1039/D1NH00079A. URL http://xlink.rsc.org/?DOI=D1NH00079A.
[198] S. Bao, D. Kim, C. Onwukaeme, S. Gupta, K. Saraswat, K.H. Lee, Y. Kim, D. Min, Y. Jung, H. Qiu, H. Wang, E.A. Fitzgerald, C.S. Tan, D. Nam, Low-threshold optically pumped lasing in highly strained germanium nanowires, Nat. Commun. 8 (1) (2017) 1–7, https://doi.org/10.1038/s41467-017-02026-w, 1 8, https://www.nature.com/articles/s41467-017-02026-w. URL.
[199] G. Koblmüller, B. Mayer, T. Stettner, G. Abstreiter, J.J. Finley, GaAs–AlGaAs core–shell nanowire lasers on silicon: invited review, Semicond. Sci. Technol. 32 (5) (2017), 053001, https://doi.org/10.1088/1361-6641/aa5e45. URL, http://stacks.iop.org/0268-1242/32/i=5/a=053001?key=crossref.ba4e12afb515deb7c083b6a69d81604c.
[200] C.Z. Ning, What is laser? IEEE J. Sel. Top. Quant. Electron. 85287 (c) (2013) 1–5. URL, http://www.hk-phy.org/articles/laser/laser_e.html#note.
[201] R.-M. Ma, R.F. Oulton, Applications of nanolasers, Nat. Nanotechnol. 14 (1) (2019) 12–22, https://doi.org/10.1038/s41565-018-0320-y. URL, https://doi.org/10.1038/s41565-018-0320-y, http://www.nature.com/articles/s41565-018-0320-y.
[202] R.F. Oulton, V.J. Sorger, T. Zentgraf, R.M. Ma, C. Gladden, L. Dai, G. Bartal, X. Zhang, Plasmon lasers at deep subwavelength scale, Nature 461 (7264) (2009) 629–632, https://doi.org/10.1038/nature08364. URL, http://www.nature.com/articles/nature08364.
[203] B. Mayer, D. Rudolph, J. Schnell, S. Morkötter, J. Winnerl, J. Treu, K. Müller, G. Bracher, G. Abstreiter, G. Koblmüller, J.J. Finley, Lasing from individual GaAs-AlGaAs core-shell nanowires up to room temperature, Nat. Commun. 4 (1) (2013) 2931, https://doi.org/10.1038/ncomms3931. URL, http://www.nature.com/doifinder/10.1038/ncomms3931, http://www.nature.com/ncomms/2013/131205/ncomms3931/full/ncomms3931.html, http://www.nature.com/articles/ncomms3931.
[204] Y. Ding, Q. Yang, X. Guo, S. Wang, F. Gu, J. Fu, Q. Wan, J. Cheng, L. Tong, Nanowires/microfiber hybrid structure multicolor laser, Opt Express 17 (24) (2009) 21813–21818, https://doi.org/10.1364/OE.17.021813. URL, http://www.osapublishing.org/oe/abstract.cfm?URI=oe-17-24-21813.

[205] Q. Yang, X. Jiang, X. Guo, Y. Chen, L. Tong, Hybrid structure laser based on semiconductor nanowires and a silica microfiber knot cavity, Appl. Phys. Lett. 94 (10) (2009), 101108, https://doi.org/10.1063/1.3093821. URL, http://aip.scitation.org/doi/10.1063/1.3093821.
[206] W. Wei, Y. Liu, X. Zhang, Z. Wang, X. Ren, Evanescent-wave pumped room-temperature single-mode GaAs/AlGaAs core-shell nanowire lasers, Appl. Phys. Lett. 104 (22) (2014), 223103, https://doi.org/10.1063/1.4881266. URL http://aip.scitation.org/doi/10.1063/1.4881266.
[207] Q. Bao, W. Li, P. Xu, M. Zhang, D. Dai, P. Wang, X. Guo, L. Tong, On-chip Single-Mode CdS Nanowire Laser, vol. 12, 2020, https://doi.org/10.1038/s41377-020-0277-0. URL, http://www.nature.com/articles/s41377-020-0277-0.
[208] W.-Z. Xu, F.-F. Ren, D. Jevtics, A. Hurtado, L. Li, Q. Gao, J. Ye, F. Wang, B. Guilhabert, L. Fu, H. Lu, R. Zhang, H.H. Tan, M.D. Dawson, C. Jagadish, Vertically emitting indium phosphide nanowire lasers, Nano Lett. 18 (6) (2018) 3414–3420, https://doi.org/10.1021/acs.nanolett.8b00334. URL, https://pubs.acs.org/doi/10.1021/acs.nanolett.8b00334.
[209] A.Y. Zhizhchenko, A.B. Cherepakhin, M.A. Masharin, A.P. Pushkarev, S.A. Kulinich, A.A. Kuchmizhak, S.V. Makarov, Directional lasing from nanopatterned halide perovskite nanowire, Nano Lett. 21 (23) (2021) 10019–10025, https://doi.org/10.1021/acs.nanolett.1c03656. URL, https://doi.org/10.1021/acs.nanolett.1c03656.
[210] M. Yu, M.J. Dyer, G.D. Skidmore, H.W. Rohrs, X. Lu, K.D. Ausman, J.R.V. Ehr, R.S. Ruoff, Three-dimensional manipulation of carbon nanotubes under a scanning electron microscope, Nanotechnology 10 (3) (1999) 244, https://doi.org/10.1088/0957-4484/10/3/304. URL, https://iopscience.iop.org/article/10.1088/0957-4484/10/3/304, https://iopscience.iop.org/article/10.1088/0957-4484/10/3/304/meta.
[211] X. Ye, Y. Zhang, C. Ru, J. Luo, S. Xie, Y. Sun, Automated pick-place of silicon nanowires, IEEE Trans. Autom. Sci. Eng. 10 (3) (2013) 554–561, https://doi.org/10.1109/TASE.2013.2244082. URL, http://ieeexplore.ieee.org/document/6472260/.
[212] H. Xie, D.S. Haliyo, S. Régnier, A versatile atomic force microscope for three-dimensional nanomanipulation and nanoassembly, Nanotechnology 20 (21) (2009), 215301, https://doi.org/10.1088/0957-4484/20/21/215301. URL, https://iopscience.iop.org/article/10.1088/0957-4484/20/21/215301, https://iopscience.iop.org/article/10.1088/0957-4484/20/21/215301/meta.
[213] S. Sergent, M. Takiguchi, H. Taniyama, A. Shinya, E. Kuramochi, M. Notomi, Design of nanowire-induced nanocavities in grooved 1D and 2D SiN photonic crystals for the ultra-violet and visible ranges, Opt Express 24 (23) (2016), 26792, https://doi.org/10.1364/oe.24.026792. URL, https://www.osapublishing.org/abstract.cfm?URI=oe-24-23-26792.
[214] S. Sergent, M. Takiguchi, T. Tsuchizawa, H. Taniyama, E. Kuramochi, M. Notomi, Nanomanipulating and tuning ultraviolet ZnO- nanowire-induced photonic crystal nanocavities, ACS Photonics 4 (2017) 1040–1047, https://doi.org/10.1021/acsphotonics.7b00116.
[215] A. Hurtado, D. Jevtics, B. Guilhabert, Q. Gao, H.H. Tan, C. Jagadish, M.D. Dawson, Novel nanoscale transfer printing technique for precise positioning of nanowire lasers, SPIE Newsroom (2017) 10–12, https://doi.org/10.1117/2.1201612.006830. URL, http://www.spie.org/x124803.xml.
[216] T. Xu, S. Yang, S.V. Nair, H.E. Ruda, Nanowire-array-based photonic crystal cavity by finite-difference time-domain calculations, Phys. Rev. B 75 (12) (2007), 125104, https://doi.org/10.1103/PhysRevB.75.125104. URL, https://link.aps.org/doi/10.1103/PhysRevB.75.125104.
[217] H. Kim, W.-J.J. Lee, A.C. Farrell, J.S.D. Morales, P. Senanayake, S.V. Prikhodko, T.J. Ochalski, D.L. Huffaker, Monolithic InGaAs nanowire array lasers on silicon-on-insulator operating at room temperature, Nano Lett. 17 (6) (2017) 3465–3470, https://doi.org/10.1021/acs.nanolett.7b00384. URL, https://pubs.acs.org/doi/10.1021/acs.nanolett.7b00384, http://pubs.acs.org/doi/abs/10.1021/acs.nanolett.7b00384.
[218] B.H. Le, X. Liu, N.H. Tran, S. Zhao, Z. Mi, An electrically injected AlGaN nanowire defect-free photonic crystal ultraviolet laser, Opt Express 27 (4) (2019) 5843–5850, https://doi.org/10.1364/OE.27.005843. URL, http://www.osapublishing.org/oe/abstract.cfm?URI=oe-27-4-5843.
[219] C.-W. Tu, M. Fränzl, Q. Gao, H.-H. Tan, C. Jagadish, H. Schmitzer, H.P. Wagner, Lasing from InP nanowire photonic crystals on InP substrate, Adv. Opt. Mater. 9 (3) (2021), 2001745, https://doi.org/10.1002/ADOM.202001745. URL, https://onlinelibrary.wiley.com/doi/full/10.1002/adom.202001745 https://onlinelibrary.wiley.com/doi/abs/10.1002/adom.202001745 https://onlinelibrary.wiley.com/doi/10.1002/adom.202001745.
[220] T. Frost, S. Jahangir, E. Stark, S. Deshpande, A. Hazari, C. Zhao, B.S. Ooi, P. Bhattacharya, Monolithic electrically injected nanowire array edge-emitting laser on (001) silicon, Nano Lett. 14 (8) (2014) 4535–4541, https://doi.org/10.1021/nl5015603. URL, https://pubs.acs.org/doi/10.1021/nl5015603.
[221] M. Feng, Z. Li, J. Wang, R. Zhou, Q. Sun, X. Sun, D. Li, H. Gao, Y. Zhou, S. Zhang, D. Li, L. Zhang, J. Liu, H.-B. Wang, M. Ikeda, X. Zheng, H. Yang, Room-temperature electrically injected AlGaN-based near-ultraviolet laser grown on Si, ACS Photonics 5 (3) (2018) 699–704, https://doi.org/10.1021/acsphotonics.7b01215. URL, http://pubs.acs.org/doi/10.1021/acsphotonics.7b01215, https://pubs.acs.org/doi/10.1021/acsphotonics.7b01215.
[222] M. Rashidi, H.H. Tan, S. Mokkapati, Stable, multi-mode lasing in the strong localization regime from InP random nanowire arrays at low temperature, Optica 8 (9) (2021) 1160–1166, https://doi.org/10.1364/OPTICA.425593. URL, http://www.osapublishing.org/optica/abstract.cfm?URI=optica-8-9-1160.
[223] Q.H. Song, H. Cao, Improving optical confinement in nanostructures via external mode coupling, Phys. Rev. Lett. 105 (5) (2010), 53902, https://doi.org/10.1103/PhysRevLett.105.053902. URL, https://link.aps.org/doi/10.1103/PhysRevLett.105.053902.
[224] W.W. Wong, Z. Su, N. Wang, C. Jagadish, H.H. Tan, Epitaxially grown InP micro-ring lasers, Nano Lett. 21 (13) (2021) 5681–5688, https://doi.org/10.1021/ACS.NANOLETT.1C01411. URL, https://pubs.acs.org/doi/abs/10.1021/acs.nanolett.1c01411.
[225] S. Wirths, B.F. Mayer, H. Schmid, M. Sousa, J. Gooth, H. Riel, K.E. Moselund, Room-temperature lasing from monolithically integrated GaAs microdisks on silicon, ACS Nano 12 (3) (2018) 2169–2175, https://doi.org/10.1021/acsnano.7b07911. URL, https://pubs.acs.org/doi/10.1021/acsnano.7b07911.
[226] X. Yuan, D. Pan, Y. Zhou, X. Zhang, K. Peng, B. Zhao, M. Deng, J. He, H.H. Tan, C. Jagadish, Selective area epitaxy of III–V nanostructure arrays and networks: growth, applications, and future directions, Appl. Phys. Rev. 8 (2) (2021), 021302, https://doi.org/10.1063/5.0044706. URL, https://aip.scitation.org/doi/abs/10.1063/5.0044706.